

Non-radial oscillation modes in hybrid stars: consequences of a mixed phase

Deepak Kumar^{†,‡} Hiranmaya Mishra[†] Tuhin Malik^{*}

[‡]Indian Institute of Technology Gandhinagar, Gandhinagar 382 355, Gujarat, India

[†]Theory Division, Physical Research Laboratory, Navarangpura, Ahmedabad 380 009, India

[‡]School of Physical Sciences, National Institute of Science Education and Research, Jatni-752050, India

^{*}CFisUC, Department of Physics, University of Coimbra, P-3004 - 516 Coimbra, Portugal

E-mail: deepakk@prl.res.in, hm@prl.res.in, tuhin.malik@gmail.com

Abstract. We study the possibility of the existence of a deconfined quark matter in the core of neutron star (NS)s and its relation to non-radial oscillation modes in NSs and hybrid star (HS)s. We use relativistic mean field (RMF) models to describe the nuclear matter at low densities and zero temperature. The Nambu–Jona-Lasinio (NJL) model is used to describe the quark matter at high densities and zero temperature. A Gibbs construct is used to describe the hadron-quark phase transition (HQPT) at large densities. Within the model, as the density increases, a mixed phase (MP) appears at density about 2.5 times the nuclear matter saturation density (ρ_0) and ends at density about $5\rho_0$ beyond which the pure quark matter phase appears. It turns out that a stable HS of maximum mass, $M = 2.27M_\odot$ with radius $R = 14$ km (for NL3 parameterisation of nuclear RMF model), can exist with the quark matter in the core in a MP only. HQPT in the core of maximum mass HS occurs at radial distance, $r_c = 0.27R$ where the equilibrium speed of sound shows a discontinuity. Existence of quark matter in the core enhances the non-radial oscillation frequencies in HSs compared to NSs of the same mass. This enhancement is significantly large for the g modes. Such an enhancement of the g modes is also seen for a density dependent Bayesian (DDB) parameterisation of the nucleonic EOS. The non-radial oscillation frequencies depend on the vector coupling in the NJL model. The values of g and f mode frequencies decrease with increase the vector coupling in quark matter.

Contents

1	Introduction	1
2	Formalism	4
2.1	Equation of state for nuclear matter	4
2.2	Equation of state for quark matter	7
2.3	Hadron-quark phase transition and mixed phase	9
3	Non-radial fluid oscillation modes of compact stars	12
4	Equilibrium and adiabatic sound speeds	18
4.1	Speed of sound in hadronic phase	18
4.2	Speed of sound in quark phase	21
4.3	Speed of sound in mixed phase	22
5	Results and discussion	22
5.1	Equation of state and properties of neutron/hybrid star	22
5.2	Tidal deformability	27
5.3	Oscillation modes in hybrid stars	28
6	Summary and conclusion	32

1 Introduction

Neutron Star (NS)s are exciting cosmic laboratories to study the behavior of matter at extreme densities. The properties of NSs not only open up many possibilities related to composition, structure and dynamics of cold matter in the observable universe but also throws light on the interaction of matter at a fundamental level [1]. Such compact stars, observed as pulsars, are believed to contain matter of densities few times nuclear saturation density ($\rho_0 \simeq 0.158 \text{ fm}^{-3}$) in its core. To explain and understand the properties of such stars, one needs to connect different branches of physics like low energy nuclear physics, quantum chromodynamics (QCD) under extreme conditions, general theory of relativity (GTR) etc [2–6].

The macroscopic properties of such a compact star like its mass, radius, moment of inertia, tidal deformability in a binary merging system and different modes of oscillations etc. depend crucially on its composition that affect the variation of pressure with energy density or equation of state (EOS). Indeed, recent radio, x-ray and gravitational wave observations of NSs have provided valuable insights into the EOS of dense matter [7–9]. The observations of high mass pulsars like PSR *J1614 – 2230* ($M = 1.928 \pm 0.017 M_\odot$) [10], PSR *J0348 – 0432* ($M = 2.01 \pm 0.04 M_\odot$) [11] and PSR *J0740 + 6620* ($M = 2.08 \pm 0.07 M_\odot$) [12] and very recently PSR *J1810 + 1714* with a mass ($M = 2.13 \pm 0.04 M_\odot$) [13] have already drawn attention on nuclear interactions at high densities with questions regarding the possible presence of exotic matter in them. To constrain the nature of EOS more stringently, simultaneous measurements of NS mass and radius are essential. The precise determinations of NS radii is difficult due to inaccurate modeling the x-ray spectra emitted by the atmosphere of a NS. The high-precision x-ray space missions, such as the Neutron star Interior Composition ExploreR

(NICER) have already shed some light in this direction. Of late, NICER has come up with a measurement of the radius $12.71_{-1.19}^{+1.14}$ km, for NS with mass $1.34_{-0.16}^{+0.15} M_{\odot}$ [14], and other independent analyses show that the radius is $13.02_{-1.06}^{+1.24}$ km for an NS with mass $1.44_{-0.14}^{+0.15} M_{\odot}$ [15]. Further, the recent measurement of the equatorial circumferential radius of the highest mass ($2.072_{-0.066}^{+0.067} M_{\odot}$) pulsar PSR J0740 + 6620 is $12.39_{-0.98}^{+1.30}$ km [16, 17] by NICER will play an important role in this domain.

The core of the NS can, in principle, support various possible exotic phases of QCD. While perturbative QCD (pQCD) predicts deconfined quark matter at large densities, their applicability is rather limited in the sense that these conclusions are applicable only to very large baryon densities i.e. $\rho_B \geq 40\rho_0$ [18]. The most challenging region to study theoretically is, however, at intermediate densities i.e. few times nuclear matter saturation density which is actually relevant for the matter in the core of NSs. The first principle Lattice QCD (LQCD) calculation in this connection is also difficult due to the sign problem in lattice simulations at finite densities. At present such calculations are limited to low baryon densities only i.e. $\mu_B/T \leq 3.5$ [19]. On the otherhand, many effective models predict possibilities of various exotic phases of quark matter at such intermediate density region. These include pion superfluidity [20–22], various colour superconducting phases like 2-flavour colour superconductivity [23–25], colour flavour locked phase (CFL) [26], Larkin-Ovchinkov-Fulde-Ferrel (LOFF) [27, 28] phase, crystalline superconductivity phase etc. However, the signature of such phases in quark matter from the study of NSs have been rather challenging. The GW170817 [9] event explored the constraints on the EOS using tidal deformability extracted from the phase of the gravitational waveforms during the late stage of inspiral merger [29–34]. Though not conclusive, it is quite possible that one or both the merging NSs could be Hybrid Star (HS)s i.e. with a core of quark matter or a Mixed Phase (MP) core of quark and hadronic matter [35, 36]. Within the current observational status, it is difficult to distinguish between a canonical NS without a quark matter core from a HS with a core of pure quark matter or a core of quark matter in a MP with hadronic matter. This calls for exploring other observational signature to solve this “masquerade” problem [37, 38].

In this context, it has been suggested that the study of the non-radial oscillation modes of NSs can have the possibility of providing the compositional information regarding the matter in the interior of the NSs. This includes the NSs with a hyperon core [39–41], a quark core or a MP core with quark and hadronic matter [38, 42–47]. This is because the non-radial oscillations not only depend upon the EOS i.e. $p(\epsilon)$ but also on the derivatives $\frac{dp}{d\epsilon}$ and $\frac{\partial p}{\partial \epsilon}$ [48]. Since the appearance of hyperons does not involve any phase transition, their effects on the non-radial oscillation modes can be milder compared to a hadron-quark phase transition (HQPT) at finite densities whose effect can be more pronounced. The non-radial oscillation modes can be studied within the framework of GTR [49, 50]. Here, the fluid perturbation equations can be decomposed into spherical harmonics leading to two classes of oscillations depending upon the parity of the harmonics. The even parity oscillations produce spheroidal (polar) deformation while the odd parity oscillations produce toroidal deformation. The polar quasi-normal mode (QNM)s can further be classified into different kinds of modes depending upon the restoring force that acts on the fluid element when it gets displaced from its equilibrium position [51]. These oscillations couple to the gravitational waves and can be used as the diagnostic tools in studying the phase structure of the matter inside NSs. The important modes for this are the pressure (p) modes, fundamental (f) modes and gravity (g) modes. The frequency of the g modes is lower than that of p modes while the frequency of f modes lie in between. These are the fluid oscillation modes to be

distinguished from w modes which are associated with the perturbation of space-time metric itself [52]. In the present work, we focus on g and f modes oscillations arising from dense matter from both neutron star matter (NSM) and hybrid star matter (HSM). For nuclear matter, the existence of such low frequency g modes was shown earlier in Refs. [53, 54]. The origin of g mode is related to the convective stability i.e. stable stratification of the star. When a parcel of the fluid is displaced, the pressure equilibrium is restored rapidly through sound waves while compositional equilibrium, decided by the weak interaction takes a longer time causing the buoyancy force to oppose the displacement. This sets in the oscillations. The g mode oscillation frequencies are related to the Brunt-Väisälä frequency (ω_{BV}) which depends on the difference between the equilibrium sound speed (c_e^2) and adiabatic or the constant composition sound speed (c_s^2) i.e. $\omega_{\text{BV}}^2 \propto (1/c_e^2 - 1/c_s^2)$ as well as on the local metric. Such g modes without any phase transition have been studied earlier for the nuclear matter, hyperonic matter, superfluidity [39, 40, 55–63].

It may be mentioned that much of the recent works on the estimation of ω_{BV} are based on the parameterised form of β -equilibrated nuclear matter EOS [43, 48]. In the present work, on the otherhand, we use Relativistic Mean Field (RMF) model to estimate the ω_{BV} and use it to calculate the g modes oscillation frequencies. In the core of HSs with quark matter core (either in a MP or in a pure quark matter phase), the ω_{BV} can become large enough inside of the star at a radial distance r_c from the center where HQPT takes place and drive the g mode oscillations.

It may be noted that g modes oscillations have been studied earlier in the context of the HQPT [38, 42–48, 64]. In most of these investigations, the hadronic matter description is through a parameterized form of nuclear matter EOS and the quark matter description is through a bag model or an improved version of the same. In the present investigation, for the nuclear matter sector we use a RMF theory involving nucleons interacting with scalar and vector meson mean fields along with self-interactions of the mesons leading to reasonable saturation properties of nuclear matter. For the description of quark matter we use a two flavour Nambu–Jona-Lasinio (NJL) model where the parameters of the model are fixed from the physical variables like pion mass, pion decay constant and light quark condensate that encodes the physics of the chiral symmetry breaking. The phase transition from hadronic matter to quark matter can be considered either through a Maxwell construct or a Gibbs construct leading to a MP [65]. It ought to be noted that the kind of phase transition depends crucially on the surface tension [66–72] of the quark matter which, however, is poorly known. Gibbs construct is relevant for smaller value of surface tension while Maxwell construct becomes relevant for large values of surface tension [73, 74].

We organize this paper as follows. In section 2.1 we discuss salient features of RMF models describing the nuclear matter. Specifically, we consider two different RMF models - namely, the NL3 parameterized RMF with constant couplings along with nonlinear mesonic interactions and a RMF model with density dependent couplings of baryon meson interaction. Such a model has been quite successful in describing nuclear matter properties and finite nuclei [75]. Recently, using a Bayesian Inference framework in conjunction with minimal constraints on nuclear saturation properties, the maximum mass of neutron stars exceeding $2M_{\odot}$, and low density equation of state (EOS) calculated using chiral effective theory for pure neutron matter, the density dependent coupling parameters have been investigated [76, 77]. Such a density dependent Bayesian (DDB) model will be the other RMF model for hadronic matter that we shall use in the analysis for the HQPT. In section 2.2, we discuss the NJL model and write down the EOS for the quark matter. In section 2.3 we discuss the HQPT

using Gibbs construct when there are multiple chemical potentials to describe the system. In section 3, we discuss the stellar structure equations as well as the non-radial fluid oscillations of the compact stars. We give here, in some detail, the derivation of the pulsation equations. In section 4, we discuss the estimation of the equilibrium and adiabatic speed of sound in different phases of matter. In section 5 we discuss the results of the present investigation regarding thermodynamics of the dense matter, MP construction, HS structure and the non-radial mode oscillations. Finally in section 6, we summarize the results and give an outlook for the further investigation. We use natural units here where $\hbar = c = G = 1$.

2 Formalism

2.1 Equation of state for nuclear matter

We discuss briefly the general RMF framework to construct the EOS of the NSM in Hadronic Phase (HP). In this framework, the interaction among the baryons is realized through the exchange of mesons. We confine our analysis for the NSM constituting of baryons (neutron and proton) and leptons (electron and muon). The relevant mesons for this purpose are the σ , ω and ρ mesons [78–81]. The scalar σ mesons create a strong attractive interactions, the vector ω mesons on the otherhand are responsible for the repulsive short range interactions. The neutron and proton do only differ in terms of their isospin projections. The isovector ρ mesons are included to distinguish between baryons. The Lagrangian including baryons as the constituents of the nuclear matter and mesons as the carriers of the interactions is given as [82, 83]

$$\mathcal{L} = \sum_b \mathcal{L}_b + \mathcal{L}_l + \mathcal{L}_{\text{int}}, \quad (2.1)$$

where,

$$\mathcal{L}_b = \sum_b \bar{\Psi}_b (i\gamma_\mu \partial^\mu - q_b \gamma_\mu A^\mu - m_b + g_\sigma \sigma - g_\omega \gamma_\mu \omega^\mu - g_\rho \gamma_\mu \vec{I}_b \vec{\rho}^\mu) \Psi_b, \quad (2.2)$$

$$\mathcal{L}_l = \bar{\psi}_l (i\gamma_\mu \partial^\mu - q_l \gamma_\mu A^\mu - m_l) \psi_l, \quad (2.3)$$

$$\begin{aligned} \mathcal{L}_{\text{int}} = & \frac{1}{2} \partial_\mu \sigma \partial^\mu \sigma - \frac{1}{2} m_\sigma^2 \sigma^2 - V(\sigma) - \frac{1}{4} \Omega^{\mu\nu} \Omega_{\mu\nu} + \frac{1}{2} m_\omega^2 \omega_\mu \omega^\mu, \\ & - \frac{1}{4} \vec{R}^{\mu\nu} \vec{R}_{\mu\nu} + \frac{1}{2} m_\rho^2 \vec{\rho}_\mu \vec{\rho}^\mu - \frac{1}{4} F^{\mu\nu} F_{\mu\nu}, \end{aligned} \quad (2.4)$$

and,

$$V(\sigma) = \frac{\kappa}{3!} (g_{\sigma N} \sigma)^3 + \frac{\lambda}{4!} (g_{\sigma N} \sigma)^4. \quad (2.5)$$

Where $\Omega_{\mu\nu} = \partial_\mu \omega_\nu - \partial_\nu \omega_\mu$, $\vec{R}_{\mu\nu} = \partial_\mu \vec{\rho}_\nu - \partial_\nu \vec{\rho}_\mu$ and $F_{\mu\nu} = \partial_\mu A_\nu - \partial_\nu A_\mu$ are the mesonic and electromagnetic field strength tensors. \vec{I}_b denotes the isospin operator. The Ψ_b and ψ_l are baryon and lepton doublets. The σ , ω and ρ meson fields are denoted by σ , ω and ρ and their masses are m_σ , m_ω and m_ρ , respectively. The parameters m_b and m_l denote the vacuum masses for baryons and leptons. The meson-baryon couplings g_σ , g_ω and g_ρ are the scalar, vector and isovector coupling constants, respectively. In RMF approximation, one replaces the meson fields by their expectation values which then act as classical fields in which baryons

move *i.e.* $\langle \sigma \rangle = \sigma_0$, $\langle \omega_\mu \rangle = \omega_0 \delta_{\mu 0}$, $\langle \rho_\mu^a \rangle = \delta_{\mu 0} \delta_3^a \rho_3^0$. The mesonic equations of motion can be found by the Euler-Lagrange equations for the meson fields using the Lagrangian Eq. (2.1)

$$m_\sigma^2 \sigma_0 + V'(\sigma_0) = \sum_{i=n,p} g_\sigma n_i^s, \quad (2.6)$$

$$m_\omega^2 \omega_0 = \sum_{i=n,p} g_\omega n_i, \quad (2.7)$$

$$m_\rho^2 \rho_3^0 = \sum_{i=n,p} g_\rho I_{3i} n_i, \quad (2.8)$$

where, I_{3i} is the third component of the isospin of a given baryon. We have taken $I_{3(n,p)} = (-\frac{1}{2}, \frac{1}{2})$. The baryon density, n_B , lepton density, n_l , and scalar density, n^s , at zero temperature are given by

$$n_B = \sum_{i=n,p} \frac{\gamma k_{Fi}^3}{6\pi^2} \equiv \sum_{i=n,p} n_i, \quad (2.9)$$

$$n_l = \frac{k_{Fl}^3}{3\pi^2}, \quad (2.10)$$

and

$$n^s = \frac{\gamma}{(2\pi)^3} \sum_{i=n,p} \int_0^{k_{Fi}} \frac{m^*}{E(k)} d^3k \equiv \sum_{i=n,p} n_i^s, \quad (2.11)$$

where, $E(k) = \sqrt{m^{*2} + k^2}$ being the single particle energy for nucleons with a medium dependent mass given as

$$m^* = m_b - g_\sigma \sigma_0. \quad (2.12)$$

Further, $k_{Fi} = \sqrt{\tilde{\mu}_i^2 - m^{*2}}$ is the Fermi momenta of the nucleons defined through an effective baryonic chemical potential, $\tilde{\mu}_i$ given as

$$\tilde{\mu}_i = \mu_i - g_\omega \omega_0 - g_\rho I_{3i} \rho_3^0. \quad (2.13)$$

Similarly, k_{Fl} is the leptonic Fermi momenta *i.e.* $k_{Fl} = \sqrt{\mu_l^2 - m_l^2}$. Further $\gamma = 2$ correspond to the spin degeneracy factor for nucleons and leptons and μ_l denotes the chemical potential for leptons.

The total energy density, ϵ_{HP} , within the RMF model is given by

$$\begin{aligned} \epsilon_{\text{HP}} &= \frac{m^{*4}}{\pi^2} \sum_{i=n,p} H(k_{Fi}/m^*) + \sum_{l=e,\mu} \frac{m_l^4}{\pi^2} H(k_{Fl}/m_l) \\ &+ \frac{1}{2} m_\sigma^2 \sigma_0^2 + V(\sigma_0) + \frac{1}{2} m_\omega^2 \omega_0^2 + \frac{1}{2} m_\rho^2 \rho_3^0{}^2. \end{aligned} \quad (2.14)$$

The pressure, p_{HP} , can be found using the thermodynamic relation as

$$p_{\text{HP}} = \sum_{i=n,p,l} \mu_i n_i - \epsilon_{\text{HP}}. \quad (2.15)$$

Table 1. The nucleon masses (m_b), σ meson mass (m_σ), ω meson mass (m_ω), ρ meson mass (m_ρ) and couplings g_σ , g_ω , g_ρ , κ , λ in NL3 parameterisation [84].

Parameters	Values
m_b (MeV)	939
m_σ (MeV)	508.194
m_ω (MeV)	782.501
m_ρ (MeV)	763.000
g_σ^2	104.387
g_ω^2	165.585
g_ρ^2	79.6
κ (fm $^{-1}$)	3.86
λ	-0.0159

Table 2. The nucleon masses (m_b), meson masses, m_i ($i = \sigma, \omega, \rho$) and coupling constants g_{i0} , a_i ($i = \sigma, \omega, \rho$) and the saturation nuclear density n_0 in DDB model [76, 77].

Parameters	Values
m_b (MeV)	939
m_σ (MeV)	508.194
m_ω (MeV)	782.501
m_ρ (MeV)	763.000
a_σ	0.071
a_ω	0.046
a_ρ	0.666
$g_{\sigma 0}$	9.690
$g_{\omega 0}$	11.756
$g_{\rho 0}$	8.281
n_0 (fm $^{-3}$)	0.147

In Eq. (2.14) we have introduced the function $H(z)$ which is given as

$$H(z) = \frac{1}{8} \left[z\sqrt{1+z^2}(1+2z^2) - \sinh^{-1} z \right], \quad (2.16)$$

In the present investigation, we consider two different parameterisation for the nucleonic EOS - (i) the NL3 parameterisation of RMF model as discussed in Ref. [84]. The corresponding parameters are listed in Table 1. The other parameterisation of the RMF model is DDB [76, 77] consistent with the phenomenology of the saturation properties of nuclear matter as well as the gravitational wave data regarding tidal deformation [9]. In case of DDB, the couplings are density dependent and defined as

$$g_\sigma = g_{\sigma 0} e^{-(x^{a_\sigma}-1)}, \quad (2.17)$$

$$g_\omega = g_{\omega 0} e^{-(x^{a_\omega}-1)}, \quad (2.18)$$

$$g_\rho = g_{\rho 0} e^{-a_\rho(x-1)}, \quad (2.19)$$

where, $x = n_B/n_0$. The DDB parameters g_{i0} , a_i , ($i = \sigma, \omega, \rho$) and n_0 are given in Table 2. In DDB parameterisation, the cubic and quartic terms in Eq. (2.1) are taken to be zero so that $V(\sigma) = 0$. We mention here that these parameter set lies within the the 90 percent confidence inference (CI) of the $R_{1.4}$ of NS with mass $1.4M_\odot$ as analysed in Ref. [76, 77]

Due to the density dependent couplings, the effective baryon chemical potential as in Eq. (2.13) gets redefined as

$$\tilde{\mu}_i = \mu_i - g_\omega \omega_0 - g_\rho I_{3i} \rho_3^0 - \Sigma^r, \quad (2.20)$$

where, Σ^r is the ‘‘rearrangement term’’ which is given as [75]

$$\Sigma^r = \sum_{i=n,p} \left\{ -\frac{\partial g_\sigma}{\partial n_B} \sigma_0 n_i^s + \frac{\partial g_\omega}{\partial n_B} \omega_0 n_i + \frac{\partial g_\rho}{\partial n_B} \rho_3^0 I_{3i} n_i \right\}. \quad (2.21)$$

The NSs are globally charge neutral as well as the matter inside the core is under β -equilibrium. So the chemical potentials and the number densities of the constituents of NSM are related by the following equations,

$$\mu_i = \mu_B + q_i \mu_E, \quad (2.22)$$

$$\sum_{i=n,p,l} n_i q_i = 0, \quad (2.23)$$

where, μ_B and μ_E are the baryon and electric chemical potentials and q_i is the charge of the i^{th} particle.

2.2 Equation of state for quark matter

We note down here, for the sake of completeness, the salient features of the thermodynamics of NJL model with two flavours that we use to describe the EOS of the quark matter. The Lagrangian of the model with four point interactions is given by

$$\begin{aligned} \mathcal{L} = & \bar{\psi}_q (i\gamma^\mu \partial_\mu - m_q) \psi_q + G_s [(\bar{\psi}_q \psi_q)^2 + (\bar{\psi}_q i\gamma^5 \tau \psi_q)^2] \\ & + G_v [(\bar{\psi}_q \gamma^\mu \psi_q)^2 + (\bar{\psi}_q i\gamma^\mu \gamma^5 \tau \psi_q)^2]. \end{aligned} \quad (2.24)$$

Here, ψ_q is the doublet of u and d quarks. We have also taken here a current quark mass, m_q which is that we have taken as same for u and d quarks. The second term describes the four point interactions in the scalar and pseudo-scalar channel. The third term is a phenomenological vector interaction giving rise to repulsive interaction for $G_v > 0$ which can make the EOS stiffer. Except for the explicit symmetry breaking term proportional to current quark mass, the Lagrangian is chirally symmetric. Using the standard method of thermal field theory one can write down the thermodynamic potential Ω within a mean field approximation at a given temperature, ($T = \beta^{-1}$) and quark chemical potential, ($\mu_q = \mu_B/3$) [85] as

$$\begin{aligned} \Omega(M, T, \mu) = & -2N_c \sum_{i=u,d} \int \frac{d\mathbf{k}}{(2\pi)^3} \times \left\{ E_k + \frac{1}{\beta} \log (1 + \exp (-\beta(E_k - \tilde{\mu}_i))) \right. \\ & \left. + \frac{1}{\beta} \log (1 + \exp (-\beta(E_k + \tilde{\mu}_i))) \right\} + G_s \rho_s^2 - G_v \rho_v^2. \end{aligned} \quad (2.25)$$

Where, $N_c = 3$ is the colour degrees of freedom and $E_k = \sqrt{\mathbf{k}^2 + M^2}$ is the on shell single particle energy of the quark with constituent quark mass M and $\tilde{\mu}_i$ being an effective quark chemical potential in the presence of the vector interaction. The constituent quark mass, M , satisfies the mass gap equation

$$M = m_q - 2G_s \rho_s, \quad (2.26)$$

and the effective quark chemical potential satisfies

$$\tilde{\mu}_i = \mu_i - 2G_v \rho_v. \quad (2.27)$$

Here, we focus our attention to $T = 0$ which is applicable to the cold NSs. Using the relation $\lim_{\beta \rightarrow \infty} \frac{1}{\beta} \log (e^{-\beta x} + 1) = -x \Theta(-x)$, the thermal factors in Eq. (2.25) go over into step functions and the mean field thermodynamic potential Eq. (2.25) becomes in the limit $T \rightarrow 0$

$$\Omega(M, 0, \mu) = -2N_c \sum_{i=u,d} \int \frac{d\mathbf{k}}{(2\pi)^3} \left\{ E_k + (\tilde{\mu}_i - E_k) \Theta(\tilde{\mu}_i - E_k) \right\} + G_s \rho_s^2 - G_v \rho_v^2. \quad (2.28)$$

The scalar density, ρ_s , and vector density, ρ_v , are given as

$$\begin{aligned}\rho_s &= -2N_c \sum_{i=u,d} \int \frac{d\mathbf{k}}{(2\pi)^3} \frac{M}{E_k} \left(1 - \Theta(\tilde{\mu}_i - E_k)\right) \\ &= -\frac{N_c M^3}{\pi^2} \sum_{i=u,d} \left[G(\Lambda/M) - G(k_{Fi}/M) \right],\end{aligned}\quad (2.29)$$

and

$$\rho_v = 2N_c \sum_{i=u,d} \int \frac{d\mathbf{k}}{(2\pi)^3} \Theta(\tilde{\mu}_i - E_k) = 2N_c \sum_{i=u,d} \frac{k_{Fi}^3}{6\pi^2}.\quad (2.30)$$

In Eq. (2.29), we have introduced the function $G(z)$ which is defined as

$$G(z) = \frac{1}{2} \left[z\sqrt{1+z^2} - \tanh^{-1} \left(\frac{z}{\sqrt{1+z^2}} \right) \right].\quad (2.31)$$

The difference of the vacuum energy densities between the non-perturbative vacuum (characterized by the constituent quark mass, M) and energy density of the perturbative vacuum (characterized by current quark mass, m_q) is the bag constant, B , i.e.

$$B = \Omega(M, T = 0, \mu = 0) - \Omega(m_q, T = 0, \mu = 0).\quad (2.32)$$

This bag constant is to be subtracted from Eq. (2.28) so that the thermodynamic potential vanishes at vanishing temperature and density. The pressure, p_{NJL} , i.e. the negative of the thermodynamic potential of the quark matter in NJL model is given as

$$p_{\text{NJL}} = p_{\text{vac}} + p_{\text{med}} + B,\quad (2.33)$$

where the vacuum, p_{vac} , and the medium, p_{med} , contributions to the pressure are given by

$$p_{\text{vac}} = \frac{4N_c}{(2\pi)^3} \int_{|k| \leq \Lambda} d\mathbf{k} \sqrt{\mathbf{k}^2 + M^2} \equiv \frac{2N_c}{\pi^2} M^4 H(\Lambda/M),\quad (2.34)$$

and,

$$\begin{aligned}p_{\text{med}} &= \frac{2N_c}{(2\pi)^3} \sum_{i=u,d} \int_0^{k_{Fi}} d\mathbf{k} \left[\sqrt{\mathbf{k}^2 + M^2} - \tilde{\mu}_i \right] + G_s \rho_s^2 - G_v \rho_v^2 \\ &= \frac{N_c}{\pi^2} \sum_{i=u,d} M^4 \left[H(k_{Fi}/M) - \tilde{\mu}_i \rho_i \right] + G_s \rho_s^2 - G_v \rho_v^2,\end{aligned}\quad (2.35)$$

where, $k_{Fi} = \Theta(\tilde{\mu}_i - M) \sqrt{\tilde{\mu}_i^2 - M^2}$ is the fermi-momenta of $i = u, d$ quark and Λ is the three momentum cut-off. The function $H(z)$ is already defined in Eq. (2.16). From the thermodynamic relation, the energy density, ϵ_{NJL} , is given as

$$\epsilon_{\text{NJL}} = \sum_{i=u,d} \mu_i \rho_i - p_{\text{NJL}}.\quad (2.36)$$

where, $\rho_i = \frac{\gamma k_{Fi}^3}{6\pi^2}$, ($i = u, d, e$) with the degeneracy factor $\gamma = 6$ for quarks and $\gamma = 2$ for electron. NSM is charge neutral as well as β -equilibrated. So the chemical potentials of the u and d quarks can be expressed in terms of quark chemical potential, μ_q , and electric chemical potential, μ_E , as $\mu_i = \mu_q + q_i \mu_E$ ($i = u, d$). q_i 's are the electric charges of u and d quarks. The condition of charge neutrality is

$$\frac{2}{3}\rho_u - \frac{1}{3}\rho_d - \rho_e = 0. \quad (2.37)$$

Since the typical electric charge chemical potential is of the order of MeV, one can neglect the electron mass so that $k_{Fe} = |\mu_e|$. The total pressure and the energy density for the charge neutral quark matter are then given by

$$p_{QP} = p_{NJL} + p_e, \quad (2.38)$$

$$\epsilon_{QP} = \epsilon_{NJL} + \epsilon_e, \quad (2.39)$$

where, $\epsilon_e \simeq \frac{\mu_e^4}{4\pi^2}$ and $p_e \simeq \epsilon_e/3$.

We may note that NJL model has four parameters – namely, the current quark mass, m_q , the three momentum cutoff, Λ , and the two coupling constants, G_s and G_v . The values of the parameters are usually chosen by fitting the pion decay constant, $f_\pi = 92.4$ MeV, the chiral condensate, $\langle -\bar{\psi}_q \psi_q \rangle_u = \langle -\bar{\psi}_q \psi_q \rangle_u = (240.8 \text{ MeV})^3$ and the pion mass, $m_\pi = 135$ MeV. This fixes $m_q = 5.6$ MeV, $G_s \Lambda^2 = 2.44$ and $\Lambda = 587.9$ MeV. As mentioned G_v is not fitted from any other physical constraint and we take it as a free parameter. We shall show our results for the two values of G_v namely $G_v = 0$ and $G_v = 0.2G_s$. With this parameterisation, the constituent quark mass, M , comes 400 MeV, the critical chemical potential, μ_c for the chiral transition turns out to be $\mu_c = 1168$ MeV for the vector coupling constant $G_v = 0$ in NJL model.

2.3 Hadron-quark phase transition and mixed phase

The baryon number density or the quark chemical potential at which the hadronic-quark phase transition occurs is not known precisely from the first principle calculations in QCD but it is expected from various model calculations to occur at a density which is few times the nuclear matter saturation density. In the context of NSs, two types of phase transitions can be possible depending upon the surface tension [66–72] of the quark matter. If the surface tension is large then there will be sharp interface and one can have a Maxwell construct for the phase transition. On the otherhand, if the surface tension is small we can have a Gibbs construct for the phase transition, where there is a MP of nuclear and quark matter. It ought to be mentioned, however, the estimated values of the surface tension for quark matter vary over a wide range and is very much model dependent. As the value of the surface tension is not precisely known yet both the scenarios, (Maxwell and Gibbs) are plausible. We adopt here the Gibbs construct for the HQPT as nicely outlined in Ref. [86]. In this case, one can achieve the charge neutrality with a positively charged hadronic matter mixed with a negatively charged quark matter in necessary amount leading to a global charge neutrality where the pressures of the both phases are the functions of two independent chemical potentials μ_B and μ_E . The Gibbs condition for the equilibrium at the zero temperature between the two phases for such a two component system is given by [65]

$$p_{HP}(\mu_B, \mu_E) = p_{QP}(\mu_B, \mu_E) = p_{MP}(\mu_B, \mu_E), \quad (2.40)$$

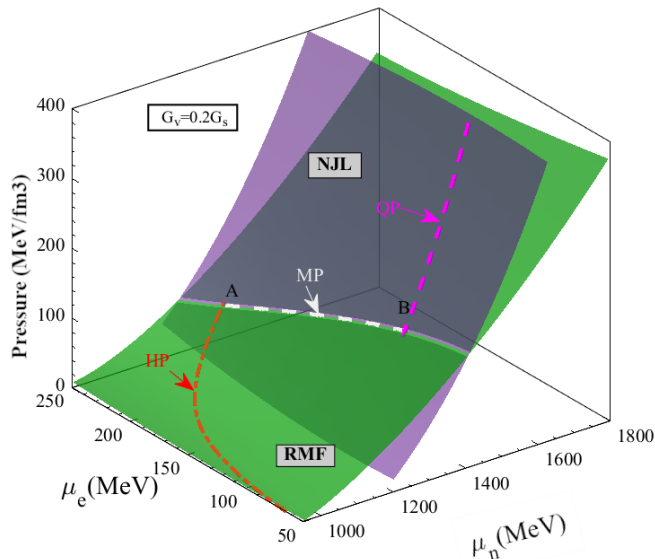


Figure 1. Pressure is plotted as a function of $\mu_n(\mu_B)$ and $\mu_e(-\mu_E)$ for HP and QP. The green surface is for HP and the purple surface is for the QP. The two surfaces intersect along the curve AB . The along the dashed portion on this line, the electrical charge neutrality is maintained. Along the red dashed line and magenta dashed line charge neutrality is maintained in HP and QP respectively. The quark matter fraction χ increases monotonically from $\chi = 0$ to $\chi = 1$ along the curve AB . We have considered here the NL3 parameterisation of RMF for the description of HP matter.

where, the pressure for HP, p_{HP} , is given in Eq. (2.15) and the pressure for the Quark Phase (QP), p_{QP} , is written down in Eq. (2.38). In Fig. 1 we illustrate this calculation, where the pressure is plotted as a function of baryon chemical potential, $\mu_B(= \mu_n)$, and the electric chemical potential, $-\mu_E(= \mu_e)$. The green surface denotes the pressure in the HP estimated from the RMF model using NL3 parameters. The purple surface denotes the pressure in the QP estimated in NJL model. The two surfaces intersect along the curve AB satisfying the global charge neutrality condition,

$$\chi \rho_c^{\text{QP}} + (1 - \chi) \rho_c^{\text{HP}} = 0, \quad (2.41)$$

where, ρ_c^{HP} and ρ_c^{QP} denote the total charge densities in HP and QP respectively and χ defines the volume fraction of the quark matter in MP defined as,

$$\chi = \frac{V_{\text{QP}}}{V_{\text{QP}} + V_{\text{HP}}}. \quad (2.42)$$

Explicitly, for a given μ_B , we calculate the electric charge chemical potential μ_E such that the pressure in both the phases are equal satisfying the Gibbs condition Eq. (2.40). This gives the intersection line (AB) of the two surfaces as shown in Fig. 1. Further imposing the global charge neutrality condition Eq. (2.41) one obtains the volume fraction χ occupied by the quark matter in MP. Thus along the line AB in Fig. 1, the volume fraction occupied by quark matter increases monotonically from $\chi = 0$ to $\chi = 1$. This gives the pressure for the charge neutral matter in MP. Below $\chi < 0$, EOS corresponds to the charge neutral

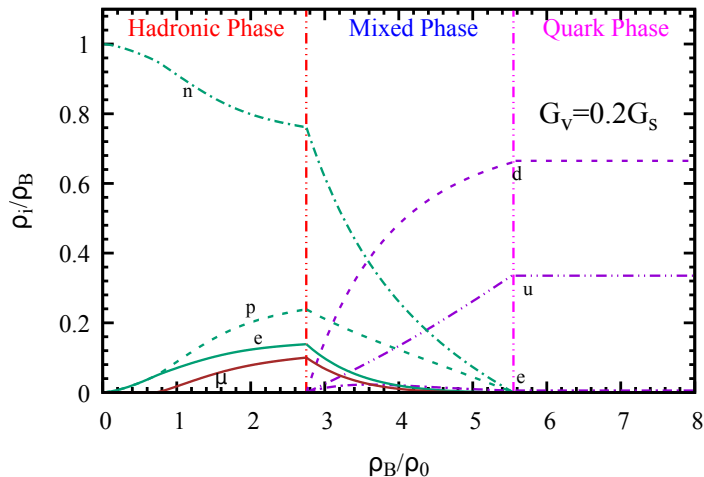


Figure 2. The particle fractions normalized with respect to baryon density for the charge neutral matter are plotted as a function of the baryon number density. The plot is for $G_v = 0.2G_s$. At $\rho_B = 2.75\rho_0$ the quark matter starts appearing and at $\rho_B = 5.72\rho_0$ the hadronic matter melts completely to the quark matter. The HP is described by RMF model with NL3 parameterisation.

hadronic matter EOS shown as the red dash curve while for $\chi > 1$ EOS corresponds to the charge neutral quark matter EOS shown as the purple dash curve in Fig. 1. With the present parametrisation of the RMF model for hadronic matter and NJL model for the quark matter, MP starts at $(\mu_B, \mu_e, p) = (1423\text{MeV}, 289.26\text{MeV}, 144.56\text{MeV}/\text{fm}^3)$ and ends at $(\mu_B, \mu_e, p) = (1597\text{MeV}, 102.40\text{MeV}, 266.23\text{MeV}/\text{fm}^3)$. This corresponds to the starting of MP at baryon density $\rho_B = 2.75\rho_0$ and ending of MP at baryon density $\rho_B = 5.72\rho_0$. For NJL model we have taken here $G_v = 0.2G_s$. For $G_v = 0$, MP starts little earlier i.e. $\rho_B = 2.36\rho_0$ and ends at $\rho_B = 5.22\rho_0$. After MP, as baryon density increases the matter is in pure charge neutral QP. We can find the energy density in the MP as follows,

$$\epsilon_{\text{MP}} = \chi\epsilon_{\text{QP}} + (1 - \chi)\epsilon_{\text{HP}}. \quad (2.43)$$

We display the particle content as a function of density for the charge neutral matter for $G_v = 0.2G_s$ in Fig. 2. In the HP, the neutron density dominates with a small fraction of proton and a small fraction of electron is also appeared to get the charge neutral HP. At $\rho_B \sim 2.76\rho_0$, the MP starts and the nucleon fraction decreases while quark fraction start increasing. Finally, at densities $\rho_B \sim 5.56\rho_0$ and above, the pure QP takes over with d-quark densities roughly becoming twice that of the u-quarks to maintain the global charge neutrality.

Similar to Eq. (2.43) the baryon number density in MP

$$\rho_{\text{MP}}^B = \chi\rho_{\text{QP}}^B + (1 - \chi)\rho_{\text{HP}}^B. \quad (2.44)$$

In MP region, nuclear matter fraction decreases while quark matter fraction increases with increasing ρ_B . As ρ_B increases further the nuclear matter melts completely to quark matter which occurs for densities beyond $\rho_B = 5.72\rho_0$.

MP construction using DDB parameterisation of the hadronic EOS is also similar except that the MP starts at $(\mu_B, \mu_e, p, \rho_B) = (1416.5\text{ MeV}, 204.58\text{ MeV}, 181.76\text{ MeV}/\text{fm}^3, 3.93\rho_0)$ and ends at $(\mu_B, \mu_e, p, \rho_B) = (1504\text{ MeV}, 108.42\text{ MeV}, 245.51\text{ MeV}/\text{fm}^3, 6.98\rho_0)$ beyond which we find QP as the stable phase.

3 Non-radial fluid oscillation modes of compact stars

In this section, we outline the equations governing the oscillation modes of the fluid comprising NSM. The most general metric for a spherically symmetric space-time is given by

$$\begin{aligned} ds^2 &= g_{\alpha\beta} dx^\alpha dx^\beta \\ &= e^{2\nu} dt^2 - e^{2\lambda} dr^2 - r^2(d\theta^2 + \sin^2\theta d\phi^2), \end{aligned} \quad (3.1)$$

where, ν and λ are the metric functions. It is convenient to define the mass function, $m(r)$ in the favour of λ as

$$e^{2\lambda} = \left(1 - \frac{2m}{r}\right)^{-1}. \quad (3.2)$$

Starting from the line element Eq. (3.1) one can obtain the equations governing the structure of spherical compact objects, the Tolman-Oppenheimer-Volkoff (TOV) equations, as

$$\frac{dp}{dr} = -(\epsilon + p) \frac{d\nu}{dr}, \quad (3.3)$$

$$\frac{dm}{dr} = 4\pi r^2 \epsilon, \quad (3.4)$$

$$\frac{d\nu}{dr} = \frac{m + 4\pi r^3 p}{r(r - 2m)}. \quad (3.5)$$

In the above set of equations ϵ , p are the energy density and the pressure respectively. $m(r)$ is the mass of the compact star enclosed within a radius r . To solve these equations, one has to supplement these equations with an equation relating pressure and energy density *i.e.* an EOS. Further, one has to set the boundary conditions at the center and surface as

$$m(0) = 0 \quad \text{and} \quad p(0) = p_c, \quad (3.6)$$

$$p(R) = 0, \quad (3.7)$$

$$e^{2\nu(R)} = 1 - \frac{2M}{R}, \quad (3.8)$$

where, the total mass of the compact object is given by $M = m(R)$ ¹, R being its radius which is defined as the radial distance where the pressure vanishes while integrating out Eqs. (3.3, 3.4 and 3.5) from the center to the surface of the star. One can solve these equations along with a boundary conditions Eqs. (3.6, 3.7 and 3.8) for a set of central densities ϵ_c or corresponding pressure p_c to obtain the mass-radius, $(M - R)$ curve.

For the sake of completeness, we give below a succinct derivation of pulsating equations in the context of NS within a relativistic setting [53, 87]. The Einstein field equation that relates the curvature of space time to the energy momentum tensor is given as

$$R_{\alpha\beta} - \frac{1}{2}g_{\alpha\beta}R = 8\pi T_{\alpha\beta}, \quad (3.9)$$

with $T_{\alpha\beta}$ being the stress energy tensor, which for a perfect fluid is given by

$$T^{\mu\nu} = (p + \epsilon)u^\mu u^\nu - pg^{\mu\nu}, \quad (3.10)$$

¹In this section, M denotes the mass of the compact stars to be distinguished from the constituent quark mass defined in Sec 2.2.

with p and ϵ being the pressure and energy density respectively and u^μ is the four-velocity. Taking (covariant) divergence of the Einstein equation, Eq. (3.9), the left hand side of Eq. (3.9) vanishes using Bianchi identity leading to covariant conservation equation of the energy momentum tensor i.e. $T_{;\mu}^{\mu\nu} = 0$. With $T^{\mu\nu}$ given in Eq. (3.10), this reduces to

$$(p + \epsilon)u^\mu u_{\nu;\mu} = \partial_\nu p - u_\nu u^\mu \partial_\mu p \quad (3.11)$$

which is the relativistic Euler equation [87]. Next, to derive the equation of motion, we use the conservation of baryon number. This is similar to using continuity equation in non-relativistic case which follows from mass conservation. The baryon number conservation equation is given by

$$\frac{dn}{d\tau} = -n u_{;\mu}^\mu, \quad (3.12)$$

where, n is the baryon number density.

We shall derive the equations in spherical coordinates and the perturbations will be expanded in terms of vector spherical harmonics. The position (t, r, θ, ϕ) of a fluid element in space time as a function of proper time τ is given by the position four-vector $\xi(\tau)$ as

$$\xi(\tau) = \begin{pmatrix} \xi^t \\ \xi^r \\ \xi^\theta \\ \xi^\phi \end{pmatrix}. \quad (3.13)$$

Consider a fluid element located at ξ_0 as its equilibrium position is displaced to $\xi(\xi_0, \tau) = \xi_0 + \zeta(\xi_0, \tau)$. This results perturbation in pressure p , in energy density ϵ and in baryon number density n as

$$p = p_0 + \delta p, \quad (3.14)$$

$$\epsilon = \epsilon_0 + \delta \epsilon, \quad (3.15)$$

$$n = n_0 + \delta n, \quad (3.16)$$

where, the subscript ‘0’ refers to the corresponding quantities in equilibrium. To derive the equations of motion for the perturbation, one has to linearize the Euler equation, Eq. (3.11) in the perturbation. For this we need the four velocities of the fluid elements $u^\mu = \frac{d\xi^\mu}{d\tau} = \frac{d\zeta^\mu}{d\tau}$. Further, we shall confine ourselves to performing the analysis for spherical harmonic component with the azimuthal index $m = 0$. For the displacement vector ζ^μ we take the ansatz

$$\begin{pmatrix} \zeta^t \\ \zeta^r \\ \zeta^\theta \\ \zeta^\phi \end{pmatrix} = \begin{pmatrix} t \\ \frac{e^{-\lambda} Q(r, t)}{r^2} P_l(\cos \theta) \\ -\frac{Z(r, t)}{r^2} \partial_\theta P_l(\cos \theta) \\ 0 \end{pmatrix}, \quad (3.17)$$

where, $Q(r, t)$ and $Z(r, t)$ are the perturbing functions. We choose a harmonic time dependence for the perturbation *i.e.* $\propto e^{i\omega t}$ with frequency ω . Further, we do not consider here toroidal deformations. From the normalisation condition for the velocity $u_\mu u^\mu = 1$, and keeping up to linear terms in the perturbation, we have $u^t = d\zeta^t/d\tau = e^{-\nu}$. The other components

of the four-velocity are given as

$$\begin{pmatrix} u^t \\ u^r \\ u^\theta \\ u^\phi \end{pmatrix} = \begin{pmatrix} e^{-\nu} \\ e^{-\nu} \dot{\zeta}^r \\ e^{-\nu} \dot{\zeta}^\theta \\ 0 \end{pmatrix}, \quad (3.18)$$

where, the dot on the perturbed coordinate denotes the derivative with respect to time ‘ t ’. Similarly, the contravariant velocity components are given using the metric given in Eq. (3.1) and Eq. (3.18) as

$$\begin{pmatrix} u_t \\ u_r \\ u_\theta \\ u_\phi \end{pmatrix} = \begin{pmatrix} e^\nu \\ -e^{2\lambda-\nu} \dot{\zeta}^r \\ -r^2 e^{-\nu} \dot{\zeta}^\theta \\ 0 \end{pmatrix}. \quad (3.19)$$

Now we simplify the Euler equation *i.e.* Eq. (3.11) by substituting the expressions for pressure, energy density and the fluid four-velocity and linearize in terms of the perturbing functions. The $\nu = t$ component of the Euler equation, Eq. (3.11), reduces to

$$(p_0 + \epsilon_0)\nu'(r) = -p'_0(r), \quad (3.20)$$

where, the superscript ‘prime’ corresponds to derivative with respect to ‘ r ’. To obtain Eq. (3.20), we have used in the LHS of Eq. (3.11), with $\nu = t$, $u^\mu u_{t;\mu} = \nu' \dot{\zeta}^r$ and in RHS we have used the fact that p_0 is isotropic so that $\dot{p}_0 - u_t u^\mu \partial_\mu p \sim -\dot{\zeta}^r p'_0(r)$. Let us recognise that the Eq. (3.20) is essentially a part of the TOV equations (Eq. (3.3)) relating pressure gradient and the metric function gradient. Next, the $\nu = r$ component of the Euler equation, Eq. (3.11), reduces to

$$\omega^2(\epsilon_0 + p_0)e^{2(\lambda-\nu)}\dot{\zeta}^r - (\delta\epsilon + \delta p)\nu'(r) - \frac{d}{dr}(\delta p) = 0. \quad (3.21)$$

Similarly, the $\nu = \theta$ component of the Euler equation, Eq. (3.11), by using $u^\mu u_{\theta;\mu} = u^t \partial_t u_\theta = -e^{-2\nu} r^2 \ddot{\zeta}^\theta$, is given as

$$\omega^2(\epsilon_0 + p_0)e^{-2\nu} r^2 \dot{\zeta}^\theta - \partial_\theta \delta p = 0. \quad (3.22)$$

Having written down the Euler equation to linear order in the perturbation, let us next consider the baryon number conservation equation *i.e.* Eq. (3.12). With the velocity components given in Eqs. (3.18, 3.19) and Eq. (3.17) for the perturbation, the number conservation equation, Eq. (3.12) can be written in terms of the radial and azimuthal perturbing functions $Q(r)$ and $Z(r)$ as

$$\frac{dn}{d\tau} = -\frac{n}{r^2} \left[e^{-(\lambda+\nu)} \frac{\partial^2 Q(r, t)}{\partial r \partial t} + e^{-\nu} l(l+1) \dot{Z} \right] P_l(\cos \theta). \quad (3.23)$$

We might note here that, since the proper time derivative is taken along the world line of the fluid parcel, we can write $\frac{dn}{d\tau} = \frac{d\Delta n}{d\tau}$, where, Δn is the Lagrangian perturbation. Further, using the relation $\partial/\partial t = e^{-\nu} \partial/\partial \tau$, we can integrate Eq. (3.23) over $d\tau$ to obtain the Lagrangian perturbation in number density Δn in terms of the perturbing functions Q and Z as

$$\frac{\Delta n}{n_0} = -\frac{1}{r^2} \left[e^{-\lambda} Q' + l(l+1)Z \right] P_l(\cos \theta). \quad (3.24)$$

To write down the equations in terms of the perturbing functions $Q(r)$ and $Z(r)$, we need to express the energy density perturbation $\delta\epsilon$ and pressure perturbation δp occurring in Eqs. (3.20, 3.21) in terms of the functions $Q(r)$ and $Z(r)$. The strategy is to use the Euler equation Eq. (3.11) to write $\delta\epsilon$ in terms of δn and use definition of bulk modulus ($\kappa = n \frac{\Delta p}{\Delta n}$) to write δp in terms of δn . One can then use the baryon number conservation equation Eq. (3.23) to write $\delta\epsilon$ and δp in terms of the perturbing functions.

Thus, using the Euler equation Eq. (3.11) to eliminate $u_{;\mu}^{\mu}$ in the baryon number conservation Eq. (3.12), we have

$$\frac{dn}{d\tau} = \frac{n}{p + \epsilon} \frac{\partial\epsilon}{\partial\tau}, \quad (3.25)$$

which leads to

$$\Delta\epsilon \simeq \frac{\epsilon_0 + p_0}{n_0} \Delta n. \quad (3.26)$$

Further, using the relation between the Lagrangian perturbation and the Eulerian perturbation i.e. $\Delta\epsilon = \delta\epsilon + \zeta^r \frac{d\epsilon_0}{dr}$ and using Eq. (3.24), we have

$$\delta\epsilon = - \left[\frac{\epsilon_0 + p_0}{r^2} \left\{ e^{-\lambda} Q' + l(l+1)Z \right\} + \frac{e^{-\lambda}}{r^2} Q \frac{d\epsilon_0}{dr} \right] P_l(\cos\theta). \quad (3.27)$$

Next, let us find out the relation between δp and Δn . The Eulerian variation δp and the Lagrangian variation Δp are related as

$$\delta p = \Delta p - \zeta^r \frac{dp_0}{dr}. \quad (3.28)$$

Thus, using Eq. (3.17) and Eq. (3.24), we have

$$\delta p = - \left[\frac{\kappa}{r^2} (e^{-\lambda} Q' + l(l+1)Z) + \frac{e^{-\lambda}}{r^2} \frac{dp_0}{dr} Q \right] P_l(\cos\theta). \quad (3.29)$$

Further, Δp is related to Δn , through bulk modulus κ i.e.

$$\kappa = n \frac{\Delta p}{\Delta n}.$$

In the relativistic Cowling approximation, the metric perturbations are neglected. This will mean the energy and pressure perturbations should also vanish. In the relativistic Cowling approximation, the energy density perturbation $\delta\epsilon$ is set to zero but pressure perturbation is not set to zero. As shown in Ref.[53], such an approximation leads to qualitatively correct result which we shall also follow. Setting $\delta\epsilon = 0$ in Eq. (3.21), and using Eq. (3.29), we have

$$\nu' \delta p + \frac{d\delta p}{dr} = -\nu' \kappa X - \frac{d(\kappa X)}{dr} - \nu' (p_0 + \epsilon_0) l(l+1) \frac{Z}{r^2} + (p_0 + \epsilon_0) Q \frac{d}{dr} \left(\frac{e^{-\lambda} \nu'}{r^2} \right), \quad (3.30)$$

where, we have defined for the sake of brevity $X = (e^{-\lambda} Q' + l(l+1)Z)/r^2$. Using this, the radial Euler equation, Eq. (3.21) becomes

$$\omega^2 (\epsilon_0 + p_0) e^{\lambda-2\nu} \frac{Q}{r^2} + \frac{d[\kappa X]}{dr} + \nu' \kappa X + \nu' (\epsilon_0 + p_0) l(l+1) \frac{Z}{r^2} - (\epsilon_0 + p_0) \frac{d}{dr} \left(\frac{e^{-\lambda} \nu'}{r^2} \right) = 0. \quad (3.31)$$

Similarly, the azimuthal component of the Euler equation Eq. (3.22) becomes

$$\omega^2(p_0 + \epsilon_0)e^{-2\nu}Z - \kappa X - p'_0 \frac{e^{-\lambda}Q}{r^2} = 0. \quad (3.32)$$

It can be shown that the Eq. (3.31) through a rearrangement of terms is identical to that obtained earlier by McDermott et. al. [53] with an appropriate change of factor 2 in the metric functions $\nu(r)$ and $\lambda(r)$. Few more comments here may be in order. In literature, sometimes the adiabatic index γ is used instead of κ and is defined as [42]

$$\gamma = \left(\frac{\partial \ln p_0}{\partial \ln n_0} \right)_s = \frac{n_0 \Delta p}{p_0 \Delta n} \quad (3.33)$$

so that $\kappa = \gamma p_0$. Further, the same can be related to adiabatic speed of sound as follows. By using the definition of Jacobian and standard thermodynamic relation

$$\left(\frac{\partial \ln p_0}{\partial \ln n_0} \right)_s = \frac{n_0^2}{p_0 \chi_{\mu\mu}} \quad (3.34)$$

in the zero temperature limit. The adiabatic speed of sound at zero temperature is defined as [88]

$$c_s^2 = \left(\frac{\partial p_0}{\partial \epsilon_0} \right)_s = \frac{n}{\mu \chi_{\mu\mu}}$$

so that

$$\gamma = \frac{p_0 + \epsilon_0}{p_0} c_s^2. \quad (3.35)$$

Let us note that Eq. (3.31) is a second order differential equation for the perturbing function $Q(r)$. We now use Eq. (3.32) to write down two coupled first order equation for the perturbing functions. Using Eq. (3.32) and Eq. (3.35), we have the equation for perturbation as

$$Q' - \frac{1}{c_s^2} \left[\omega^2 r^2 e^{\lambda-2\nu} Z + \nu' Q \right] + l(l+1)e^\lambda Z = 0. \quad (3.36)$$

Next one can calculate the combination $d[Eq.(3.32)]/dr + [Eq.(3.31)]$ and substitute Eq. (3.32) again which leads to the first order differential equation for Z' as

$$Z' - 2\nu'Z + e^\lambda \frac{Q}{r^2} - \nu' \left(\frac{1}{c_e^2} - \frac{1}{c_s^2} \right) \left(Z + \nu' e^{-\lambda+2\nu} \frac{Q}{\omega^2 r^2} \right) = 0. \quad (3.37)$$

In the above equation $c_e^2 = \frac{dp_0}{d\epsilon_0} = \frac{p'_0}{\epsilon'_0}$ is the equilibrium speed of sound. It may be noted that Eq. (3.40) can be rewritten as

$$\omega^2 e^\lambda \frac{Q}{r^2} + \omega^2 Z' + A_- e^\lambda \omega^2 Z - A_+ e^{2\nu} \frac{p'_0}{p_0 + \rho_0} \frac{q}{r^2} = 0. \quad (3.38)$$

where, $A_+ = e^{-\lambda}(\epsilon'_0/(p_0 + \epsilon_0) + \nu'/c_s^2)$ and $A_- = A_+ - 2\nu'e^{-\lambda}$. It is reassuring to see that the Eq. (3.36) and Eq. (3.38) are identical to the corresponding equations Eq.(3b) and Eq.(4a) given in Ref. [53]. The gravity mode (g mode) oscillation frequencies are closely related to the Brunt-Väisälä frequency, ω_{BV} [53]. The relativistic generalisation of ω_{BV} is given by

$$\omega_{BV}^2 = \nu'^2 e^{2\nu} \left(1 - \frac{2m}{r} \right) \left(\frac{1}{c_e^2} - \frac{1}{c_s^2} \right). \quad (3.39)$$

This also reduces to the expression for the ω_{BV} in Newtonian limit [54].

The equation for the perturbation function $Z(r)$ can be rewritten in terms of the Brunt-Väisälä frequencies as

$$Z' - 2\nu'Z + e^\lambda \frac{Q}{r^2} - \frac{\omega_{BV}^2 e^{-2\nu}}{\nu' \left(1 - \frac{2m}{r}\right)} \left(Z + \nu' e^{-\lambda+2\nu} \frac{Q}{\omega^2 r^2} \right) = 0. \quad (3.40)$$

The two coupled first order differential equations for the perturbing functions $Q(r, t)$ and $Z(r, t)$, Eqs. (3.36), (3.40), are to be solved with appropriate boundary conditions at the center and the surface. Near the center of the compact stars the behavior of the functions $Q(r)$ and $Z(r)$ are given by [42]

$$Q(r) = Cr^{l+1} \quad \text{and} \quad Z(r) = -Cr^l/l \quad (3.41)$$

where, C is an arbitrary constant and l is the order of the oscillation. The other boundary condition is the vanishing of the Lagrangian perturbation pressure, i.e. $\Delta p = 0$ at the stellar surface. Using equations Eqs. (3.28, 3.29 and 3.36), we have the Lagrangian perturbation pressure Δp given as

$$\Delta p = -\frac{(p_0 + \epsilon_0)}{r^2} \left[\omega^2 r^2 e^{\lambda-2\nu} Z + \nu' Q \right] e^{-\lambda}. \quad (3.42)$$

Thus the vanishing of Δp at the surface of the star ($r = R$) leads to the boundary condition [89]

$$\omega^2 r^2 e^{\lambda-2\nu} Z + \nu' Q \Big|_{r=R} = 0. \quad (3.43)$$

Further, in case one considers stellar models with a discontinuity in the energy density, one has to supplement additional condition at the surface of discontinuity demanding Δp to be continuous *i.e.* $\Delta p(r = r_{c-}) = \Delta p(r = r_{c+})$. Where, r_c is the radial distance of the surface of energy density discontinuity from the center. This leads to [42, 89]

$$Q_+ = Q_-, \quad (3.44)$$

$$Z_+ = \frac{e^{2\nu}}{\omega^2 r_c} \left\{ \frac{\epsilon_{0-} + p_0}{\epsilon_{0+} + p_0} \left(\omega^2 r_c^2 e^{-2\nu} Z_- + e^{-\lambda} \nu' Q_- \right) - e^{-\lambda} \nu' Q_+ \right\}, \quad (3.45)$$

where, the $-(+)$ subscript corresponds to the quantities before(after) the surface of discontinuity. In case of a Maxwell construct for phase transition, there is a discontinuity in energy density while in Gibbs construct of phase transition the energy density is continuous at the phase boundary as considered here.

With these boundary conditions the problem becomes an eigen-value problem for ' ω '. To calculate the eigen frequencies ω , we proceed as follows. For a given central density ϵ_c , we first solve the TOV equations Eqs. (3.3 - 3.5) to get the profile of the unperturbed metric functions $\lambda(r)$, $\nu(r)$ and also the mass M and the radius R of the spherical star. For a given ω , we solve the pulsating equations Eqs. (3.36 and 3.40) to determine the fluid perturbing functions $Q(r)$ and $Z(r)$ as a function of r . To solve these equations, we take the initial values for Q and Z consistent with Eq. (3.41). Specifically we took C of the order 1. The solutions of Q and Z are independent of this choice. We then calculate LHS of Eq. (3.43). The value of ω is then varied such that the boundary condition, Eq. (3.43), is satisfied. This gives the

frequency, ω as function of mass and radius. It may be noted that there can be multiple solutions of ω satisfying the pulsating equations and the boundary conditions corresponding to different initial trial values for ω . These different solutions for ω correspond to frequencies of different modes of oscillations of the compact star.

4 Equilibrium and adiabatic sound speeds

In this section we discuss both equilibrium and adiabatic sound speeds which are needed to solve the pulsating equations Eqs. (3.36) and (3.40). We present the expressions of both sound speeds for matter in HP, QP and MP. The equilibrium speed of sound is given by

$$c_e^2 = \frac{dp}{d\epsilon} = \frac{dp/dr}{d\epsilon/dr}. \quad (4.1)$$

where, p and ϵ are the total pressure and energy density. The equilibrium sound speed in NS can be evaluated numerically as a function of radial distance from the center of the star while keeping the NSM in β -equilibrium. Using the above definition (4.1), we find the equilibrium speed of sound in HP, QP and MP.

The characteristic time scale of the QNM is about 10^{-3} sec which is much smaller than the β -equilibrium time scale. Therefore, during the oscillations the composition of the matter can be assumed to be constant. Such adiabatic approximation means the adiabatic speed of sound corresponds to the constant composition i.e.

$$c_s^2 = \left(\frac{\partial p}{\partial \epsilon} \right)_{y_i} = \frac{(\partial p / \partial n_B)_{y_i}}{(\partial \epsilon / \partial n_B)_{y_i}}, \quad (4.2)$$

where, $y_i = (n_i/n_B)$'s are the fractions of the constituents of the matter which need to be held fixed while taking the derivatives. Once the derivatives are taken, we apply the β -equilibrium condition and get the adiabatic speed of sound in different phases. In the following subsections we present the analytical expressions for the adiabatic speeds of sound in HP, QP and MP.

4.1 Speed of sound in hadronic phase

In the following we estimate the adiabatic speed of sound of hadronic matter within the RMF model as

$$c_{s,\text{HP}}^2 = \frac{\left(\frac{\partial p_{\text{HP}}}{\partial n_B} \right)_{y_i}}{\left(\frac{\partial \epsilon_{\text{HP}}}{\partial n_B} \right)_{y_i}}. \quad (4.3)$$

The total energy density and total pressure of matter in HP are given in Eqs. (2.14) and (2.15). Using these equations we find the partial derivative of pressure and energy density with respect to baryon number density at constant composition (fixed y_i) as

$$\left(\frac{\partial p_{\text{HP}}}{\partial n_B} \right)_{y_i} = \sum_{i=n,p,l} \left[\mu_i y_i + \left(\frac{\partial \mu_i}{\partial n_B} \right)_{y_i} n_B \right] - \left(\frac{\partial \epsilon_{\text{HP}}}{\partial n_B} \right)_{y_i}, \quad (4.4)$$

and,

$$\begin{aligned} \left(\frac{\partial \epsilon_{\text{HP}}}{\partial n_B} \right)_{y_i} = & \frac{1}{2\pi^2} \sum_{i=n,p,e,\mu} \left[E_{F_i} k_{F_i}^2 \left(\frac{\partial k_{F_i}}{\partial n_B} \right)_{y_i} + m^* (E_{F_i} k_{F_i} - m^{*2} \log x_i) \left(\frac{\partial m^*}{\partial n_B} \right)_{y_i} \right] \\ & + (m_\sigma^2 \sigma_0 + V'(\sigma_0)) \left(\frac{\partial \sigma_0}{\partial n_B} \right)_{y_i} + m_\omega^2 \omega_0 \left(\frac{\partial \omega_0}{\partial n_B} \right)_{y_i} + m_\rho^2 \rho_3^0 \left(\frac{\partial \rho_3^0}{\partial n_B} \right)_{y_i}. \end{aligned} \quad (4.5)$$

Here, $x_i = \frac{E_{Fi} + k_{Fi}}{m^*}$. The derivatives of the meson fields at constant composition, using Eqs. (2.6-2.8) are given as

$$\left(\frac{\partial\sigma_0}{\partial n_B}\right)_{y_i} = \frac{g_\sigma(a_p + a_n)}{m_\sigma^2 + V''(\sigma_0) - g_\sigma(b_p + b_n)}, \quad (4.6)$$

$$\left(\frac{\partial\omega_0}{\partial n_B}\right)_{y_i} = \frac{g_\omega(y_p + y_n)}{m_\omega^2}, \quad (4.7)$$

$$\left(\frac{\partial\rho_3^0}{\partial n_B}\right)_{y_i} = \frac{g_\rho(y_p - y_n)}{2m_\rho^2}, \quad (4.8)$$

where, $V''(\sigma_0)$ is the second derivative of Eq. (2.5) with respect to σ_0 . The quantities a_i and b_i , ($i = n, p$) are given by

$$a_i = \frac{m^* y_i}{E_{Fi}}, \quad (4.9)$$

$$b_i = \frac{g_\sigma}{2\pi^2} \left[3m^{*2} \log x_i - E_{Fi} k_{Fi} - \frac{2m^{*2} k_{Fi}}{E_{Fi}} \right]. \quad (4.10)$$

Eqs. (4.4 and 4.5) lead, inturn, to the derivatives of the medium dependent mass (m^*) and the chemical potential (μ_i) with respect to baryon number density at constant composition is given as

$$\left(\frac{\partial m^*}{\partial n_B}\right)_{y_i} = -g_\sigma \left(\frac{\partial\sigma_0}{\partial n_B}\right)_{y_i}, \quad (4.11)$$

$$\left(\frac{\partial\mu_i}{\partial n_B}\right)_{y_i} = \left(\frac{\partial\tilde{\mu}_i}{\partial n_B}\right)_{y_i} + g_\omega \left(\frac{\partial\omega_0}{\partial n_B}\right)_{y_i} + g_\rho I_{3i} \left(\frac{\partial\rho_{30}}{\partial n_B}\right)_{y_i}, \quad (4.12)$$

where, $\tilde{\mu}_i = \sqrt{k_{Fi}^2 + m^{*2}}$. Further, we have on direct evaluation, using $n_B = \sum_{i=n,p} \frac{k_{Fi}^3}{3\pi^2}$,

$$\left(\frac{\partial k_{Fi}}{\partial n_B}\right)_{y_i} = \frac{k_{Fi}}{3n_B}. \quad (4.13)$$

Thus the partial derivatives of pressure, Eq. (4.4) and energy density Eq. (4.5) gets completely defined. This gives the adiabatic speed of sound in hadronic matter in the RMF model.

Similarly, one can determine the sound speeds in DDB model. The expressions of the partial derivatives of pressure and energy density in DDB model are similar to Eq. (4.4) and Eq. (4.5) except that there are additional terms due to the density dependent couplings. Here we give the expressions with the incorporation of corresponding changes arising from the density dependent couplings. The derivatives of the meson fields in DDB model is given as follows

$$\left(\frac{\partial\sigma_0}{\partial n_B}\right)_{y_i} = \frac{1}{m_\sigma^2 - g_\sigma(b_p + b_n)} \left(g_\sigma(a'_p + a'_n) + \left(\frac{\partial g_\sigma}{\partial n_B}\right)_{y_i} (n_p^s + n_n^s) \right), \quad (4.14)$$

$$\left(\frac{\partial\omega_0}{\partial n_B}\right)_{y_i} = \frac{1}{m_\omega^2} \left(g_\omega(y_p + y_n) + \left(\frac{\partial g_\omega}{\partial n_B}\right)_{y_i} (n_p + n_n) \right), \quad (4.15)$$

$$\left(\frac{\partial\rho_3^0}{\partial n_B}\right)_{y_i} = \frac{1}{2m_\rho^2} \left(g_\rho(y_p - y_n) + \left(\frac{\partial g_\rho}{\partial n_B}\right)_{y_i} (n_p - n_n) \right), \quad (4.16)$$

where, with a_i and b_i as given in Eqs. (4.9 and 4.10),

$$a'_i = a_i + \frac{b_i \sigma_0}{g_\sigma} \left(\frac{\partial g_\sigma}{\partial n_B} \right)_{y_i}, \quad (4.17)$$

and, the derivatives of the density dependent couplings are given as

$$\left(\frac{\partial g_\sigma}{\partial n_B} \right)_{y_i} = -\frac{g_\sigma a_\sigma}{\rho_0} x^{a_\sigma - 1}, \quad (4.18)$$

$$\left(\frac{\partial g_\omega}{\partial n_B} \right)_{y_i} = -\frac{g_\omega a_\omega}{\rho_0} x^{a_\omega - 1}, \quad (4.19)$$

$$\left(\frac{\partial g_\rho}{\partial n_B} \right)_{y_i} = -\frac{g_\rho a_\rho}{\rho_0}. \quad (4.20)$$

The derivatives of the medium dependent mass and the effective chemical potential at constant composition is defined as

$$\left(\frac{\partial m^*}{\partial n_B} \right)_{y_i} = -g_\sigma \left(\frac{\partial \sigma_0}{\partial n_B} \right)_{y_i} - \left(\frac{\partial g_\sigma}{\partial n_B} \right)_{y_i} \sigma_0, \quad (4.21)$$

and,

$$\begin{aligned} \left(\frac{\partial \mu_i}{\partial n_B} \right)_{y_i} &= \left(\frac{\partial \mu_i^*}{\partial n_B} \right)_{y_i} + \left(\frac{\partial g_\omega}{\partial n_B} \right)_{y_i} \omega_0 + g_\omega \left(\frac{\partial \omega_0}{\partial n_B} \right)_{y_i} \\ &+ \left(\frac{\partial g_\rho}{\partial n_B} \right)_{y_i} I_{3i} \rho_3^0 + g_\rho I_{3i} \left(\frac{\partial \rho_3^0}{\partial n_B} \right)_{y_i} + \left(\frac{\partial \Sigma^r}{\partial n_B} \right)_{y_i}. \end{aligned} \quad (4.22)$$

The last term on the RHS above is due to the extra ‘re-arrangement term’ in the effective baryon chemical potential, $\tilde{\mu}_i$, given in Eq. (2.21) and can be written as

$$\begin{aligned} \left(\frac{\partial \Sigma^r}{\partial n_B} \right)_{y_i} &= \sum_{i=p,n} \left[-\sigma_0 n_i^s \left(\frac{\partial^2 g_\sigma}{\partial n_B^2} \right)_{y_i} - \sigma_0 \left(\frac{\partial n_i^s}{\partial n_B} \right)_{y_i} \left(\frac{\partial g_\sigma}{\partial n_B} \right)_{y_i} - \left(\frac{\partial \sigma_0}{\partial n_B} \right)_{y_i} n_i^s \left(\frac{\partial g_\sigma}{\partial n_B} \right)_{y_i} \right. \\ &+ \omega_0 n_i \left(\frac{\partial^2 g_\omega}{\partial n_B^2} \right)_{y_i} + \omega_0 \left(\frac{\partial n_i}{\partial n_B} \right)_{y_i} \left(\frac{\partial g_\omega}{\partial n_B} \right)_{y_i} + \left(\frac{\partial \omega_0}{\partial n_B} \right)_{y_i} n_i \left(\frac{\partial g_\omega}{\partial n_B} \right)_{y_i} \\ &\left. + \rho_3^0 I_{3i} n_i \left(\frac{\partial^2 g_\rho}{\partial n_B^2} \right)_{y_i} + \rho_3^0 I_{3i} \left(\frac{\partial n_i}{\partial n_B} \right)_{y_i} \left(\frac{\partial g_\rho}{\partial n_B} \right)_{y_i} + \left(\frac{\partial \rho_3^0}{\partial n_B} \right)_{y_i} I_{3i} n_i \left(\frac{\partial g_\rho}{\partial n_B} \right)_{y_i} \right]. \end{aligned} \quad (4.23)$$

In the above, using Eqs. (4.18-4.20) the second derivatives of the couplings are directly given as

$$\left(\frac{\partial^2 g_\sigma}{\partial n_B^2} \right)_{y_i} = - \left(\frac{\partial g_\sigma}{\partial n_B} \right)_{y_i} \frac{a_\sigma x^{a_\sigma} - a_\sigma + 1}{x \rho_0}, \quad (4.24)$$

$$\left(\frac{\partial^2 g_\omega}{\partial n_B^2} \right)_{y_i} = - \left(\frac{\partial g_\omega}{\partial n_B} \right)_{y_i} \frac{a_\omega x^{a_\omega} - a_\omega + 1}{x \rho_0}, \quad (4.25)$$

$$\left(\frac{\partial^2 g_\rho}{\partial n_B^2} \right)_{y_i} = - \left(\frac{\partial g_\rho}{\partial n_B} \right)_{y_i} \frac{a_\rho}{\rho_0}. \quad (4.26)$$

Finally the derivative of the scalar condensate in Eq. (4.23) is given by, using Eq. (2.11)

$$\left(\frac{\partial n_i^s}{\partial n_B}\right)_{y_i} = a'_i + b_i \left(\frac{\partial \sigma_0}{\partial n_B}\right)_{y_i}. \quad (4.27)$$

Thus, the speed of sound in DDB is found using Eqs. (4.4-4.5) with the relevant derivatives in the DDB model defined in Eqs. (4.14-4.27).

4.2 Speed of sound in quark phase

In an identical manner one can estimate the adiabatic speed of sound in QP by taking the partial derivatives of total pressure and total energy density which are collected in Eqs. (2.38) and (2.39). In this subsection we present the analytic expression for the adiabatic speed of sound for the quark matter in NJL model. The partial derivatives of the pressure with respect to baryon number density using the Eq. (2.33) is given by

$$\left(\frac{\partial p_{\text{NJL}}}{\partial n_q}\right)_{y_i} = \left(\frac{\partial p_{\text{vac}}}{\partial n_q}\right)_{y_i} + \left(\frac{\partial p_{\text{med}}}{\partial n_q}\right)_{y_i}, \quad (4.28)$$

where,

$$\left(\frac{\partial p_{\text{vac}}}{\partial n_q}\right)_{y_i} = -\frac{N_c M^4}{\pi^2} \sum_{i=u,d} \left[H(z_\Lambda) \frac{4}{M} \left(\frac{\partial M}{\partial n_q}\right)_{y_i} + H'(z_\Lambda) \left(\frac{\partial z_\Lambda}{\partial n_q}\right)_{y_i} \right], \quad (4.29)$$

and,

$$\begin{aligned} \left(\frac{\partial p_{\text{med}}}{\partial n_q}\right)_{y_i} &= \frac{N_c M^4}{\pi^2} \sum_{i=u,d} \left[H(z_i) \frac{4}{M} \left(\frac{\partial M}{\partial n_q}\right)_{y_i} + H'(z_i) \left(\frac{\partial z_i}{\partial n_q}\right)_{y_i} \right] \\ &\quad - \frac{N_c}{3} \sum_{i=u,d} \left[y_i \tilde{\mu}_i + n_i \left(\frac{\partial \tilde{\mu}_i}{\partial n_q}\right)_{y_i} \right] - 2g_v n_q + 2g_s \rho_s \left(\frac{\partial \rho_s}{\partial n_q}\right)_{y_i}. \end{aligned} \quad (4.30)$$

The partial derivative of the energy density using Eq. (2.36) with respect to the baryon number density is given as

$$\left(\frac{\partial \epsilon_{\text{NJL}}}{\partial n_q}\right)_{y_i} = \sum_{i=u,d} \left[y_i \mu_i + n_i \left(\frac{\partial \mu_i}{\partial n_q}\right)_{y_i} \right] - \left(\frac{\partial p_{\text{NJL}}}{\partial n_q}\right)_{y_i}, \quad (4.31)$$

where, $z_i = k_{Fi}/M$ and $z_\Lambda = \Lambda/M$. The function $H(z)$ is given in Eq. (2.16) and $H'(z)$ is its derivative with respect to z . The derivative of the constituent mass is given by

$$\left(\frac{\partial M}{\partial n_q}\right)_{y_i} = -\frac{\frac{2N_c g_s}{\pi^2} M^2 (B_u + B_d)}{1 + \frac{2N_c g_s}{\pi^2} M^2 (A_u + A_d)} \quad (4.32)$$

where

$$A_i = 3G(z_i) - 3G(z_\Lambda) - G'(z_i)z_i + G'(z_\Lambda)z_\Lambda \quad (4.33)$$

$$B_i = G'(z_i) \frac{\partial k_{Fi}}{\partial n_q} \quad (4.34)$$

Here $i = u, d$. The function $G(z)$ is given in Eq. (2.31) and $G'(z)$ is its derivative with respect to z . Using these relations we can find the adiabatic speed of sound of quark matter in QP as

$$c_{s,\text{QP}}^2 = \frac{\left(\frac{\partial p_{\text{QP}}}{\partial n_q}\right)_{y_i}}{\left(\frac{\partial \epsilon_{\text{QP}}}{\partial n_q}\right)_{y_i}}. \quad (4.35)$$

4.3 Speed of sound in mixed phase

Once we have the expressions for the different sound speeds in HP and QP then it is state forward to get the sound speeds in MP by using the quark matter fraction χ as given in Eq. (2.42) in MP. In case of equilibrium sound speed, the total pressure and the total energy density of the MP is calculated by using the Eqs. (2.40) and (2.43). We take the numerical derivative of pressure with respect to energy density and get the equilibrium sound speed in MP. To estimate the adiabatic sound speed in MP we take the corresponding quantities in HP and QP and hence $c_{s,\text{MP}}^2$ is given as [48]

$$\frac{1}{c_{s,\text{MP}}^2} = \frac{\chi}{c_{s,\text{HP}}^2} + \frac{1-\chi}{c_{s,\text{QP}}^2} \quad (4.36)$$

5 Results and discussion

In this section, we present the structural properties and non-radial oscillations of NSs and HSs. We consider two RMF models, one with NL3 [84] parameterized and other is DDB [76, 77] for nucleonic matter EOS (see sec. 2.1) and a two flavour NJL model for the quark matter EOS (see sec. 2.2) with parameters, $(G_s\Lambda^2, \Lambda, m) = (2.24, 587.6\text{MeV}, 5.6\text{MeV})$ [85]. The MP is calculated using Gibbs construction, as outlined in sec. 2.3.

5.1 Equation of state and properties of neutron/hybrid star

In Fig. 3 we display the EOS with a Gibbs construct for the HQPT with the NJL EOS describing the QP. The left figure corresponds to the HP described by RMF with NL3 parametrisation while in right figure the HP is described by RMF with DDB parametrisation for the couplings. We note here that for the QP, the vector interaction induces additional repulsion among quarks and makes the EOS stiffer which is reflected in the left figure for the two values of G_v . As may be seen from Eq. (2.27); the effective chemical potential decreases for non vanishing and positive G_v . This results in a chiral transition occurring at a higher chemical potentials as G_v increases along with a corresponding higher critical energy density. As a matter of fact, with DDB EOS, we get a HQPT for $G_v = 0$ for stable NS/HS configuration. For $G_v = 0.2G_s$, the corresponding critical energy density is much too high to have a stable star with a quark matter core. Therefore, in all the results that follow, we consider only $G_v = 0$ for describing HSs when the corresponding HP is described by DDB EOS. In the left of Fig.3, we have plotted the MP EOS for two different vector couplings for the NJL model description while RMF with NL3 parametrisation for the HP. In the case of $G_v = 0$, the MP starts at baryon density $\rho_B \sim 2.36\rho_0$ with corresponding energy density being about $400 \text{ MeV}/\text{fm}^3$ and ends at densities $\rho_B \sim 5.22\rho_0$ with the corresponding energy density being about $1000 \text{ MeV}/\text{fm}^3$. As mentioned, increasing G_v results in a stiffer EOS with the higher G_v corresponding to a larger critical energy density at which the mixed phase starts to occur.

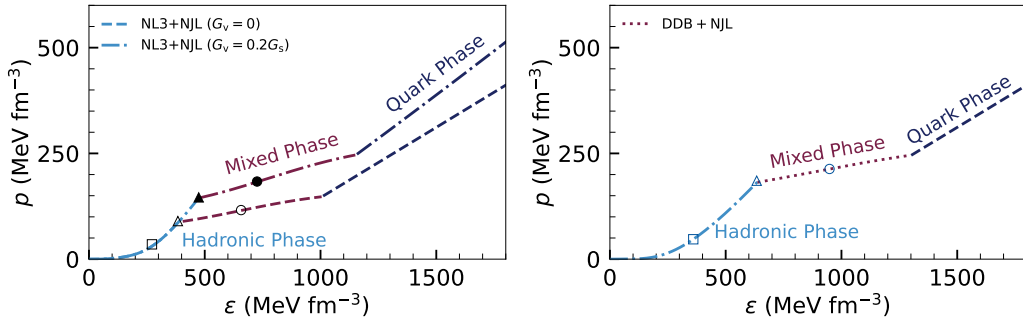


Figure 3. The EOSs of the charge neutral matter including the MP for both nuclear models in HP and the NJL model in QP. The left figure corresponds to the EOS with the NL3 parameterized hadronic matter while the right figure corresponds to the DDB parameterized hadronic matter. At high density, the NJL model is considered for the quark matter EOS with different vector couplings. In left figure, the EOSs correspond to the vector couplings $G_v = 0$ (upper curve) and $G_v = 0.2G_s$ (lower curve) in quark sector. In the right figure, the quark matter EOS corresponds to the vector coupling $G_v = 0$. In both the figures, the sky blue curve refers to the HP and the dark blue curve refers to the QP while the red curve corresponds to the MP. The open square corresponds to the central energy density of a NS of mass $1.4M_\odot$. The triangles denote the starting of the MP and correspond to NSs of mass $2.17M_\odot$ ($G_v = 0$) and $2.50M_\odot$ ($G_v = 0.2G_s$) for NL3+NJL and $2.18M_\odot$ ($G_v = 0$) for the DDB+NJL. The circles indicate the central pressure and energy density of the maximum mass stars which are $2.27M_\odot$ ($G_v = 0$) and $2.55M_\odot$ ($G_v = 0.2G_s$) for NL3+NJL and $2.20M_\odot$ ($G_v = 0$) for the DDB+NJL HSs. The pure quark matter phase is not achieved prior to the maximum mass in all the cases

In Fig. 3 (right), we show the EOS where the nuclear matter is described by the DDB model and the quark matter is described by the NJL model with $G_v = 0$. In this case, the MP starts at baryon density $\rho_B \sim 3.93\rho_0$ and ends at $\rho_B \sim 6.98\rho_0$. The open and filled circles in the EOSs denote the central energy densities of the maximum mass stars for the corresponding EOSs in Fig. 3. These circles lie in MP region indicating no pure quark matter core is realized within the present modelling of EOS. It can also be seen in Fig. 4, where we plot the quark matter fraction χ as a function of density for different G_v s and nuclear matter EOSs. The open (filled) circle in Fig. 3(left) corresponds to the maximum mass star denotes $\chi = 0.482$ (0.438) which means 48.2% (43.8%) of quark matter fraction present in the core of HS of NL3+NJL type with $G_v = 0$ ($0.2G_s$). On the otherhand, in Fig. 3 (right) the open circle correspond to the maximum mass star has $\chi = 0.506$ i.e. 50.6% of quark matter present in the core of HS of DDB+NJL in a MP. It is further observed that for the HSs considered here, there is no pure quark matter core. Quark matter is only realised in a MP in the HSs within the models considered here for the EOSs.

In Fig. 5 (left) we show the variation of the squared sound speeds, c_e^2 and c_s^2 with the normalised baryon density ρ_B/ρ_0 . On the left, we show this behaviour for the HSM described by RMF with NL3 parametrisation and NJL model. On the right the same is shown for the HSM described by RMF with DDB parametrisation and NJL model. As the density increases in the HP, the squared speeds of both the sounds increase monotonically for either cases. The maximum value of the square of speeds of sound are 0.608 in NL3+NJL model and 0.564 in DDB+NJL at the critical density after which the MP starts. In either case, the square of two sound speeds behave very differently in the MP. The square of equilibrium sound speed c_e^2 decreases discontinuously at the onset of MP to a value 0.08 (0.09) beyond which

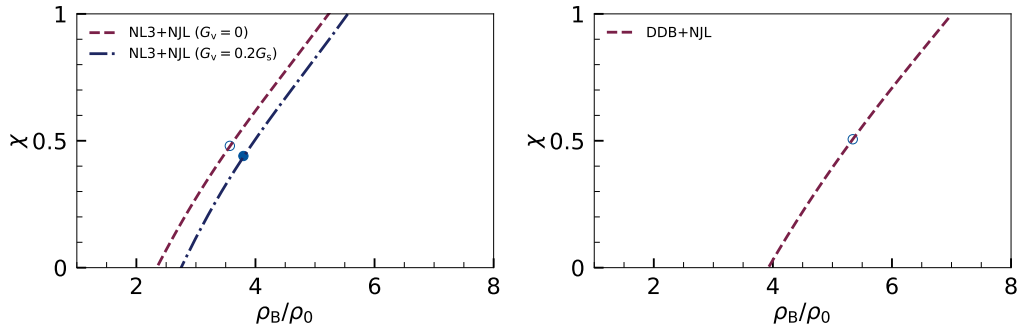


Figure 4. In the left figure, the quark fraction as a function of baryon density for the NL3 parameterized EOSs in HP and NJL model in QP while in the right figure, the quark fraction as a function of baryon density for the DDB parameterized EOS in HP and NJL model in QP as shown in Fig. 3. In the left figure, the open (dark) circle indicates the central density of the maximum mass star i.e. $\rho_{B,\text{max}} \simeq 3.5\rho_0(3.8\rho_0)$ corresponding to $M_{\text{max}} = 2.27M_\odot(2.55M_\odot)$ for $G_v = 0$ ($G_v = 0.2G_s$). In the right figure, the open circle indicates the central density of the maximum mass star i.e. $\rho_{B,\text{max}} \simeq 5.5\rho_0$

it shows a continuous behaviour till the end of MP where it again discontinuously increases from 0.06 (0.08) to 0.33 (0.33) for NL3+NJL (DDB+NJL) case. The square of the adiabatic sound speed c_s^2 , on the otherhand does not show similar discontinuous behaviour. It has an important consequence for the g modes as we shall see later. While the difference between the squared sound speeds is small in HP, at the onset of MP, this difference become large leading to large Brunt-Väisälä frequency giving rise to an enhancement of g mode frequency. We may note here that the difference between the two squared sound speeds turns out to be vanishing for the present case of two flavor NJL model. This is similar to the case of bag model EOS [38]. For massless two flavors, the charge neutrality and β -equilibrium condition renders the electron density to be constant which makes the difference between the two squared sound speeds to be vanishing. On the otherhand, this need not be the same for 3 quark flavors as the electron chemical potential $\mu_e \sim m_s^2/(4\mu_q)$ leading to electron density depending on quark mass and quark chemical potential leading to a non-vanishing value for the difference between the two speeds of sound.

Apart from enhancing the g mode frequency, the existence of the sudden rise of equilibrium sound speed has also important consequence regarding the mass and radius relation in NS. One actually needs a rise in speed of sound in a narrow region of densities, for an explanation of the compact stars to have large mass and small radius [90]. To achieve this possibility, a quarkyonic phase [90] or a vector condensate phase along with pion superfluidity [91] have been proposed recently. On the other hand, such a steep rise in the speed of sound can also arise in a MP construct within the model for hadronic matter and quark matter as used here.

In Fig. 6, we show the mass-radius relations for our models. For pure nucleonic matter the maximum mass turns out to be $2.77M_\odot$ ($2.35M_\odot$) and radius turns out to be 13.26 km (11.87 km) when the nuclear matter is describes in NL3 (DDB). If one uses MP EOS the maximum mass reduces to $2.27M_\odot$ for $G_v = 0$ with the corresponding radius $R = 14.39$ km and to $2.55M_\odot$ for $G_v = 0.2G_s$ with the radius being $R = 14.17$ km in NL3+NJL case while the same decreases to $2.20M_\odot$ with corresponding radius 12.71 km. This is essentially due to the fact that the quark matter EOS is softer compared to the nuclear mat-

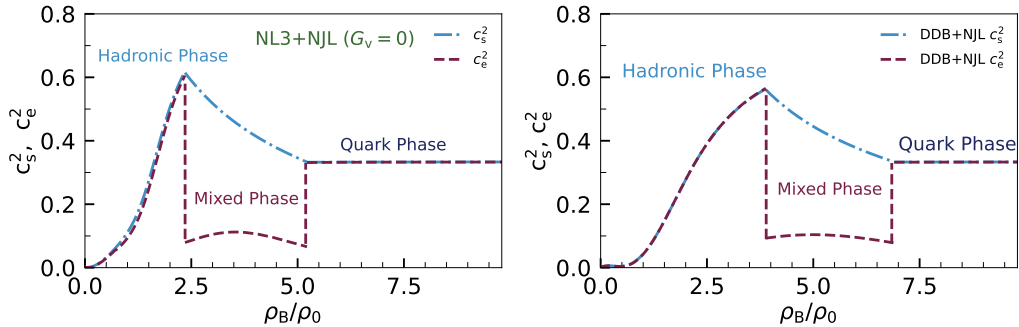


Figure 5. The variation of the square of sound speeds, (c_e^2 and c_s^2) as a function of baryon number density for the charge neutral matter. The brown dashed (blue dot-dashed) curve corresponds to the equilibrium (adiabatic) sound speed in the different phases like HP, QP and MP for the hybrid EOSs described by NL3+NJL in the left figure and DDB+NJL in the right figure. The vector coupling strength in NJL model is $G_v = 0$ in the case of the both hybrid models.

ter EOS. The central energy densities for the maximum mass HSs are $\epsilon_c^{\max} = 656 \text{ MeV/fm}^3$ ($G_v = 0$) and $\epsilon_c^{\max} = 738 \text{ MeV/fm}^3$ ($G_v = 0.2G_s$) in NL3+NJL case while $\epsilon_c^{\max} = 948 \text{ MeV/fm}^3$ ($G_v = 0$) in DDB+NJL. As central energy density is increased further, HSs become unstable i.e. $dM/d\epsilon < 0$. Thus, within the present models, we do not find stable HSs with the pure quark matter core. The quark matter, if it is present in the core, is always in MP. As G_v increases in NL3+NJL case, the MP starts at higher energy density and hence larger fraction of hadronic matter contributes to the total mass of the star as we have seen in Fig. 4 (left). This leads to an increase of the maximum mass of HS. With increasing G_v further we might expect NSs without any quark matter in the core. The radius $R_{1.4}$ for the canonical mass of $1.4M_\odot$ NSs turns out to be 14.52 km in NL3+NJL case while same turns out to be 13.21 km in DDB+NJL case. It may be noted that the x-ray pulse analysis of NICER data from PSR J0030 + 0451 by Miller et.al. found $R = 13.02_{-1.19}^{+1.14}$ km for $M = 1.44 \pm 0.15M_\odot$ [15]. Such a star will not have a quark core within these present models for the EOS of dense matter. Such a conclusion, however, should be taken with caution as this is very much dependent upon the EOSs both in hadronic and quark phase. In particular, more exotic phases of quark matter could also be possible including various color superconducting phases, various inhomogeneous phases for dense quark matter which have not been considered here.

In Fig. 7, we show the energy density and pressure profiles i.e. energy density and pressure as the functions of the radial distance from the center of the maximum mass HSs described in the present models. In the left we show for the NL3+NJL model while in the right we show for the DDB+NJL model. As mentioned earlier, the cores of the such stars are in the MP with about the 50% of quark matter and 50% of nuclear matter (see Fig. 4). The radius of the MP core is about 3.8 km (2.7 km) with the total radius of 14.17 km (12.71 km) for the HS described in NL3+NJL (DDB+NJL). We have taken here the vector coupling $G_v = 0.2G_s$ in NL3+NJL model and $G_v = 0$ in DDB+NJL model. For $G_v = 0$, in NL3+NJL, the MP core radius slightly larger i.e. 4.2 km while the star's radius being about 14.39 km. At $r = r_c$, the critical radial distance, where the matter goes from a MP to HP or vice-versa, the energy density becomes non-differentiable while pressure shows smooth behavior as may be observed in Fig. 7.

The variation of the squared sound speeds c_e^2 and c_s^2 are shown in Fig. 8 as a function of radial distance from the center of the stars for both HS as well as NS. In Fig. 8 (left) we show

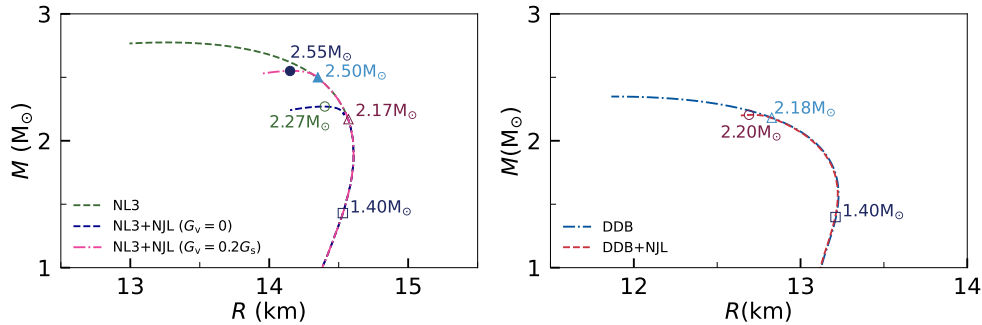


Figure 6. The mass-radius curves are plotted for the compact stars described by the models NL3, NL3+NJL in the left figure and DDB and DDB+NJL in the right figure for the different values of the vector couplings, G_v in the NJL model. In case of DDB and DDB+NJL model, the vector coupling is taken zero i.e. $G_v = 0$. The circles denote the maximum mass HSs having quark matter inside their cores for different values of vector interaction in NJL model. While the triangles represents the maximum mass NSs having hadronic matter inside the core. In the left figure, the maximum mass of HSs described by NL3+NJL hybrid model are $2.27M_\odot$ where $G_v = 0$ and $2.55M_\odot$ where $G_v = 0.2G_s$. In the right figure, the maximum mass HS described by DDB+NJL is $2.20M_\odot$.

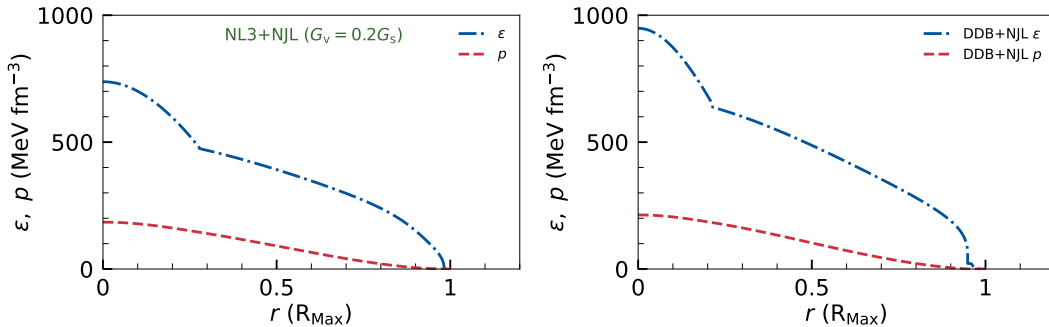


Figure 7. The energy density, ϵ (blue dot-dashed) and pressure, p (red dashed) profiles as a function of radial distance from the center of the maximum mass HSs described by the hybrid models NL3+NJL (left) and DDB+NJL (right). In case of NL3+NJL hybrid model, the vector coupling is none-zero i.e. $G_v = 0.2G_s$ while in case of DDB+NJL hybrid model, the vector coupling is zero i.e. $G_v = 0$. The transition from MP to HP happens at $\rho_B = 2.75\rho_0$ ($\rho_B = 3.95\rho_0$) corresponding with the radial distance $r_c = 0.27R_{\text{Max}}$ ($r_c = 0.21R_{\text{Max}}$) in the NL3+NJL (DDB+NJL) model.

the profiles of both c_e^2 and c_s^2 for the maximum mass stars described in NL3 and NL3+NJL models while in Fig. 8 (right) we display the same for the maximum mass stars described in DDB and DDB+NJL models. In both the cases, we have taken here $G_v = 0$. The HQPT in HSs is reflected in the variation of the square of the equilibrium sound speed, c_e^2 which changes abruptly from $c_e^2 = 0.08$ to $c_e^2 = 0.608$ in NL3+NJL model and from $c_e^2 = 0.06$ to $c_e^2 = 0.564$ for the DDB+NJL model at the critical radius r_c where the transition from a MP to a HP takes place. Such an abrupt change in c_e^2 while a smooth behaviour of c_s^2 makes the Brunt-Väisälä frequency, ($\omega_{\text{BV}}^2 \sim (c_e^{-2} - c_s^{-2})$), becoming significant at the boundary of the MP core in the HSs. As may be observed from Eq.(3.37) or Eq.(3.40), a nonvanishing ω_{BV} will affect the fluid perturbation functions $Z(r)$ and $Q(r)$ and hence will have its effect on the oscillation frequency ω . In particular this leads to an enhancement of g-mode frequencies for the HSs. We discuss more of this in subsection 5.3.

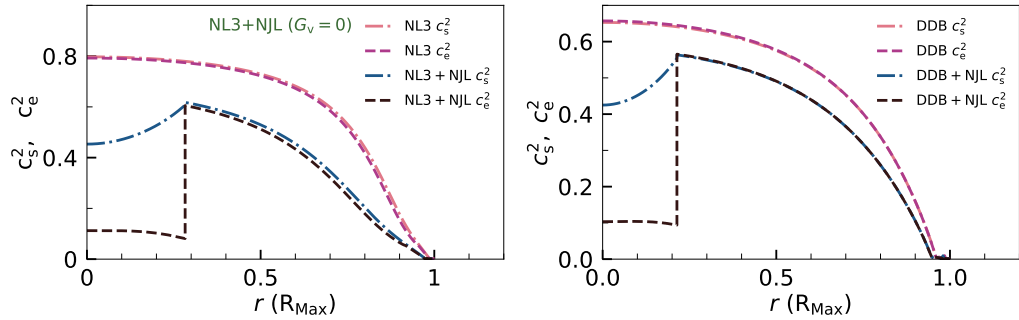


Figure 8. The equilibrium c_e^2 and the adiabatic c_s^2 sound speeds profiles inside the maximum mass stars as a function of radial distance from the center of the stars. In the left figure, the c_e^2 and c_s^2 profiles is shown as a function of the radial distance in the stars described by the NL3 and NL3+NJL models while in the right figure same in the stars described by the DDB and DDB+NJL models. The black dashed (darkblue dot-dashed) curve correspond to the c_e^2 (c_s^2) profile for the HS described by NL3+NJL (DDB+NJL) model while brown dashed (magenta dot-dashed) curve corresponds to the c_e^2 (c_s^2) profile in the NS described by NL3(DDB) model. The discontinuity in the profile of c_s^2 in the case of HSs at $r_c = 0.27R_{\text{Max}}$ ($r_c = 0.21R_{\text{Max}}$) shows the appearance of quark matter in the hybrid model NL3+NJL(DDB+NJL).

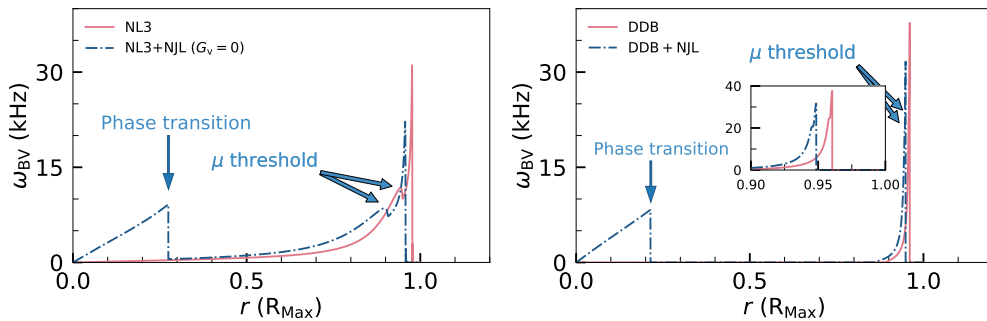


Figure 9. The Brunt-Väisälä frequency (ω_{BV}) profile in the maximum mass stars as a function of the radial distance from the center of the star. In the left figure, the ω_{BV} profile is plotted as a function of radial distance in the stars described by the NL3 and NL3+NJL model while in the right we plot same in the stars described by the DDB and DDB+NJL models. Red solid (blue dot-dashed) curve shows the ω_{BV} profile in the NS (HS where the vector coupling is considered to be zero i.e. $G_v = 0$). The little kink in the profiles near the surface of the stars shows the threshold for the appearance of muons in the all the models.

In Fig. 9 (left), we show the profile of Brunt-Väisälä frequency, ω_{BV} , in the stars of maximum masses described in NL3 and NL3+NJL while in Fig. 9 (right), we show the same described in DDB and DDB+NJL where the vector coupling $G_v = 0$ in NJL model. The steep rise of ω_{BV} at the onset of MP may be noted. The Brunt-Väisälä frequency, ω_{BV} , depends on the both the speeds of sound, see Eq. (3.39). In the core of maximum mass HS, the variation of the both sound speeds are different which is reflected in the ω_{BV} profile. The onset of muons is shown by a little kink in the figure with a slight increase in ω_{BV} .

5.2 Tidal deformability

The tidal distortion of neutron stars in a binary system links the EOS to the gravitational wave emissions during the inspiral [92]. Next we discuss the results for the tidal deformability

with the equation of state considered here. In Fig. 10 (left) shows the dimensionless tidal deformability parameters Λ_1 and Λ_2 of the NSs involved in the Binary Neutron Star (BNS) with masses m_1 and m_2 , respectively, for the hadronic EOSs DDB, NL3 and corresponding mixed phase EOS with NJL model DDB+NJL, NL3+NJL. In the GW170817 event, the chirp mass, $\mathcal{M}_{\text{chirp}} = (m_1 m_2)^{3/5} (m_1 + m_2)^{-1/5}$, was measured as $1.186 M_\odot$ [9] and these curves were calculated based on the masses involve in the BNS merger by varying m_1 in the observed range $1.365 < m_1 < 1.60$. We may note here that the quark matter core occurs for NSs of masses at around $2M_\odot$. Thus the tidal deformability Λ_1 and Λ_2 as shown in the Fig. 10 (left) will correspond to hadronic phase only. We also show the constraint imposed on $\Lambda_1 - \Lambda_2$ plane from GW170817 event in the same plot. Based on a marginalized posterior for the tidal deformability of the two binary components of GW170817, the gray solid (dot-dashed) line represents the 90%(50%) confidence interval (CI) for the tidal deformability of these two components. There are magenta solid (blue dashed) lines representing 90%(50%) confidence intervals for the constraints from GW170817: marginalized posterior using a parameterized EOS with a maximum mass requirement of at least $1.97M_\odot$. In this regard, GW170817 and its electromagnetic counterpart disfavour NL3 parameterisation of the RMF model. The DDB, however, is less stiff than NL3, so it satisfies those constraints well. The stiffness of the EOS may be attributed to either its symmetric nuclear part or its density-dependent symmetry energy. While NL3 and DDB exhibit similar symmetric nuclear matter (SNM), DDB has a softer symmetry energy than NL3. For the models NL3 and DDB, the nuclear matter incompressibility K_0 is 271 MeV, and 269 MeV and the slope of the symmetry energy L_0 is 118 MeV, 32 MeV, at saturation density respectively. Fig. 10 (right) shows the dimensionless tidal deformability as a function of NS mass of the EOS models adopted here. The blue horizontal bar indicates the 90% CI obtained for the tidal deformability of a $1.36M_\odot$ or the combined tidal deformability in the BNS for $q = m_1/m_2 = 1$ [9]. It is clear that the NL3 is outside of the 90% CI constraint whereas DDB is within the acceptable range. As discussed above the NSs masses below $2.18M_\odot$ and $2.17M_\odot$ correspond to the only hadronic phase EOSs for DDB and NL3 mixed phases EOSs, respectively. It can be seen from the figure that the tidal deformability Λ bifurcate from the same NS masses for those EOSs.

5.3 Oscillation modes in hybrid stars

We next show, here, the results for f and g modes for NSs and HSs in different models presented in this study. We shall focus our attention to the quadruple mode ($l = 2$) only. It may be expected from the coupled Eqs. (3.36 and 3.40) for the fluid perturbation functions $Q(r)$ and $Z(r)$ the two sound speeds c_s^2 and c_e^2 play an important role in the determination of different solutions for these functions and hence on the frequencies of the oscillation modes. The typical frequency of g modes lies in the range from few 100 Hz up to 1 kHz while that of f modes lies in the range 1 – 3 kHz. As mentioned in Sec. 3, we solve Eqs. (3.36 and 3.40) in a variational method to determine the oscillation frequencies. As this is computed using a variational method, the final solutions depend upon the initial guesses for the frequencies. To get a solution of the f mode, we give the initial guess for the frequency ($f = \omega/2\pi$) of the order of few kHz. On the other hand, to look for a g mode we give the initial guess for the same in the range of few hundred Hz. In Fig. 11, we show the f mode frequencies as a function of mass of compact stars for the both NS and HS described by NL3 and NL3+NJL models in the left figure while same as described by DDB and DDB+NJL model in the right figure. In the left figure, the blue curves refer to the f mode frequencies for HSs with $G_v = 0$ (blue dotted) and with $G_v = 0.2G_s$ (blue dot-dashed) while the magenta curve refers to

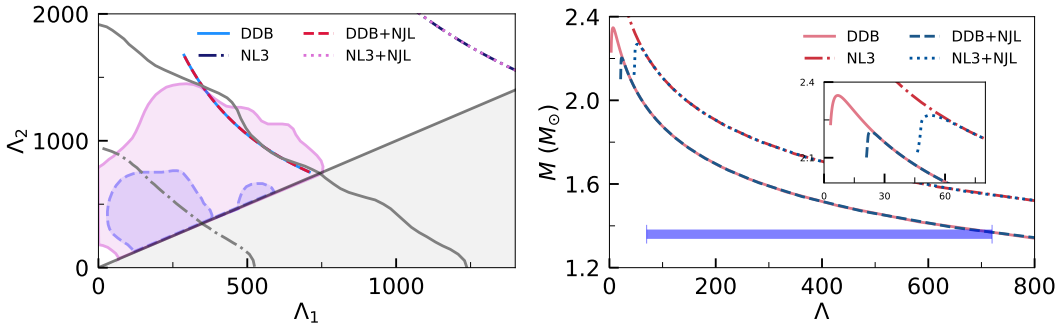


Figure 10. Based on the hadronic NL3, DDB and their hybrid EOS with NJL quark matter model for a mixed phase. (left) we show the dimensionless tidal deformability parameters Λ_1 and Λ_2 of the GW170817 binary neutron star merger, for the fixed measured chirp mass of $\mathcal{M}_{\text{chirp}} = 1.186M_\odot$. A gray solid (dot-dashed) line indicates a 90%(50%) confidence interval for the tidal deformability of GW170817’s two binary components based on their marginalized posteriors. In this figure, magenta solid (blue dashed) lines represent 90%(50%) confidence intervals for the constraints from GW170817 : marginalized posterior using a parameterized EOS and a maximum mass requirement of $1.97M_\odot$. (right) The dimensionless tidal deformability as a function of the NS mass. The tidal deformability constraint of a $1.36M_\odot$ star is represented by the blue bar in the right panel.

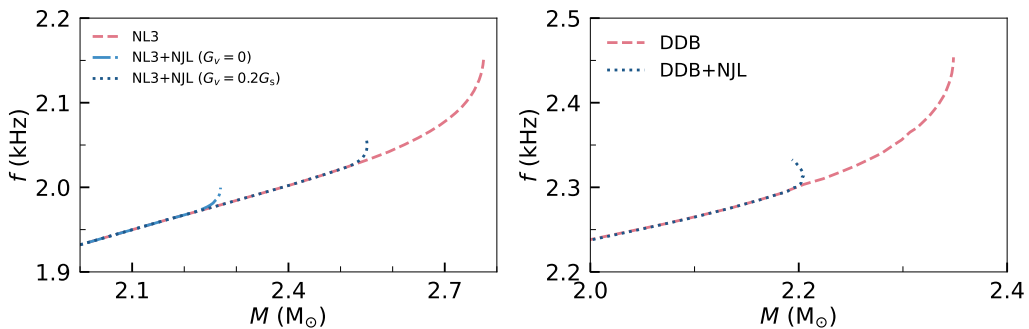


Figure 11. The oscillation frequencies of f mode $f = \omega/2\pi$ in kHz as a function of the star’s masses which are described by NL3 and NL3+NJL models in the left figure and same as a function of the star’s masses which are described by DDB and DDB+NJL models in the right figure. The magenta dashed curve corresponds to NSs i.e. without any quark matter core. (left) The blue dot-dashed (blue dotted) curves correspond to the f mode frequencies of the HSs which are described by NL3+NJL hybrid model for $G_v = 0$ ($G_v = 0.2G_s$). (right) The blue dotted curve corresponds to the f mode frequencies of the HSs which are described by DDB+NJL hybrid model for $G_v = 0$. The appearance of the quark matter in the core enhances the oscillation frequencies.

the f mode frequencies for NSs described by NL3+NJL and NL3, respectively. In the right figure, we show same as the left figure but for the DDB+NJL and DDB model, respectively where the vector coupling is zero i.e. $G_v = 0$. We may observe here that there is a mild rise in the frequencies for the f modes for stars with a quark matter core. Such a rise of non-radial oscillation frequencies due to the quark matter core was also observed in Ref. [38, 48]. However for f modes, the rise due to the quark matter in the core, is very small. *Eg.* for a HS star, described by NL3+NJL where $G_v = 0$, of mass $M = 2.27M_\odot$, the f mode frequency becomes 2 kHz from a value of 1.97 kHz of a NS of same mass.

In Fig. 12, we plot the g mode frequencies as a function of the mass of the compact

stars for the both NS and HS described by NL3 and NL3+NJL models in the left figure while same as described by DDB and DDB+NJL model in the right figure. For NSs, the compact stars without any quark matter core, the g mode frequencies lie in the range of (322 – 341) Hz (139 – 148) Hz for the stars of masses larger than $2 M_\odot$ described by NL3 (DDB) model. On the otherhand, in the presence of quark matter in MP, the frequencies rise sharply to about 589 Hz ($G_v = 0$) and 589 Hz ($G_v = 0.2G_s$) in the case of NL3+NJL model while same rises sharply to about 303 Hz ($G_v = 0$) in the case of DDB+NJL. Let us note that at the onset of the MP in case of NSs, c_e^2 decreases abruptly. This is due to the fact that the electron chemical potential falls at the onset of MP. This is due to the fact that the charge neutral nuclear matter undergoes a phase transition to one component of HP which is positively charged and the other component of QP which is negatively charged. This sudden change in the lepton number density at MP threshold leads to sudden drop of c_e^2 as shown in Fig. 8. This leads to an abrupt rise of the ω_{BV} which enhances the g mode frequency. As G_v increases the MP core decreases and hence its contribution to the g mode enhancement also decreases.

We note that the g modes that we obtained for NSs or HSs are driven by the Brunt-Väisälä frequency which quantifies the mismatch between the mechanical and chemical equilibrium rates of a displaced fluid parcel and is expressed by the local equilibrium and adiabatic speeds of sound. Such core g mode solutions in sub-kHz frequency range can also arise due to a sharp discontinuity in energy density in a first order phase transition [93, 94]. Such low frequency g modes due to quark-hadron discontinuity has also been shown to be a feature of HSs that distinguish hadronic stars or strange quark stars based on non-radial oscillation modes [43]. On the otherhand non-radial oscillation modes with a MP of quark-hadron matter was explored by Sotani etal [42]. It was shown here that including finite size effects in the mixed phase it is possible to distinguish between the existence or absence of density discontinuity in NS interior from gravitational waves of the f mode [42]. In an interesting later work of Ranea-Sandoval etal explored different non-radial oscillation modes (f , p and g modes) with an interpolating function relating hadron and quark phases unlike a Gibbs construct as has been attempted here [45]. We might note that for the phase transition considered here with NJL model, a Gibbs construct is consistent as the recent calculation using effective models like linear sigma model [68]; Polyakov quark meson model [70] as well as NJL model [69] suggest a lower value of surface tension $\sim 5 - 20\text{MeV}/\text{fm}^2$ justifying the use of a Gibbs construct.

Next, we discuss the solution of the perturbing functions $Q(r)$ and $Z(r)$. In Fig. 13, we have plotted the functions $Q(r)$ and $Z(r)$ as a function of radial distance from the center for both g and f modes. Let us first discuss the solutions of perturbing functions $Q(r)$ and $Z(r)$ for NSs. The angular function $Z(r)$ is plotted as a solid red line (Z_f) for f mode and as a solid blue line (Z_g) for g mode. For f modes, $Z(r)$ decreases monotonically starting from a vanishing value at $r = 0$ consistent with the initial condition given in Eq. (3.41). As may be clear from Eq. (3.40), for vanishing ω_{BV} , $Z'(r)$ is negative and therefore $Z(r)$ decreases as r increases. When the Brünt-Väisälä frequency, ω_{BV} becomes significant, the forth term in Eq. (3.40) starts to become important. However, if ω is large (as in the case with f modes) the contribution of the second term in the parenthesis of Eq. (3.40) is suppressed so that $Z(r)$ decreases monotonically as seen (red solid line) in Fig 13. On the otherhand, for the g mode with the lower ω , the second term in the parenthesis becomes dominant. This makes the forth term in Eq. (3.40) negative and significant near the surface as ω_{BV} becomes significant here. It turns out that the overall sign of $Z'(r)$ becomes positive near the surface resulting eventually in the change of sign of $Z(r)$ as shown (blue solid line) in Fig. 13. Thus the f

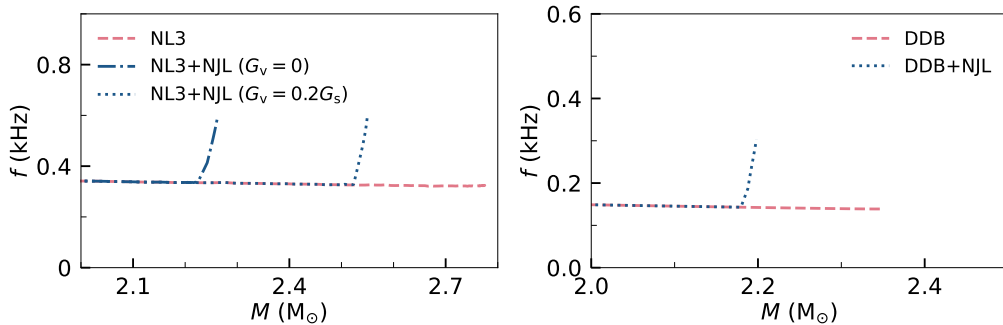


Figure 12. The oscillation frequencies of g mode $f = \omega/2\pi$ in kHz as a function of the star’s masses which are described by NL3 and NL3+NJL models in the left figure and same as a function of the star’s masses which are described by DDB and DDB+NJL models in the right figure. The magenta dashed curve corresponds to NSs i.e. without any quark matter core. (left) The blue dot-dashed (blue dotted) curves correspond to the g mode frequencies of the HSs which are described by NL3+NJL hybrid model for $G_v = 0$ ($G_v = 0.2G_s$). (right) The blue dotted curve corresponds to the g mode frequencies of the HSs which are described by DDB+NJL hybrid model for $G_v = 0$. The appearance of the quark matter in the core enhances the oscillation frequencies.

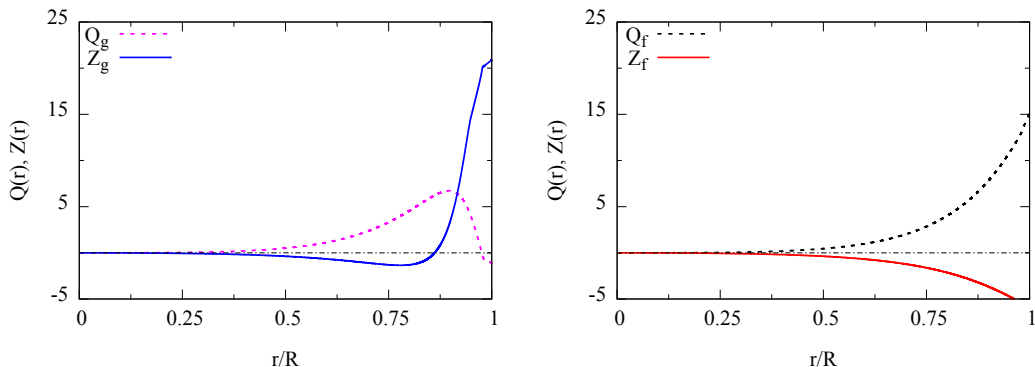


Figure 13. The solutions of the fluid perturbation functions $Q(r)$ and $Z(r)$ as a function of the radial distance for the maximum mass ($M = 2.77M_\odot$) neutron star obtained from the NL3 parameterized EOS. The solid (dashed) line corresponds to the angular function, $Z(r)$ (radial function, $Q(r)$). Both perturbing functions for f modes (Q_f and Z_f) show monotonic behavior while for g modes these function do not and have nodes near the surface of the NS.

mode shows no node for $Z(r)$, the g mode solution shows a node. We have taken through out $l = 2$. The dashed lines show the behaviour of the perturbing function $Q(r)$ as Q_f and Q_g for f and g modes respectively. Both these functions start from vanishing values and start to increase with r . $Q(r)$ for f mode (Q_f) increases monotonically while $Q(r)$ for g mode (Q_g) starts to decrease when $Z(r)$ changes sign and eventually become negative near the surface consistent with the boundary condition given in Eq. (3.43). Thus similar to $Z(r)$, $Q(r)$ also does not show any node for f modes while the solutions of the $Q(r)$ for the g modes, (Q_g) has a node near the surface.

We, next, display the perturbing functions $Q(r)$ and $Z(r)$ for HSs in Fig. 14. On the left, we show the functions $Q(r)$ and $Z(r)$ for g modes while on the right display the same functions associated with the f modes. Let us first discuss the g mode perturbing functions. We first observe that the Brunt-Väisälä frequency, ω_{BV} is significant near the center as well

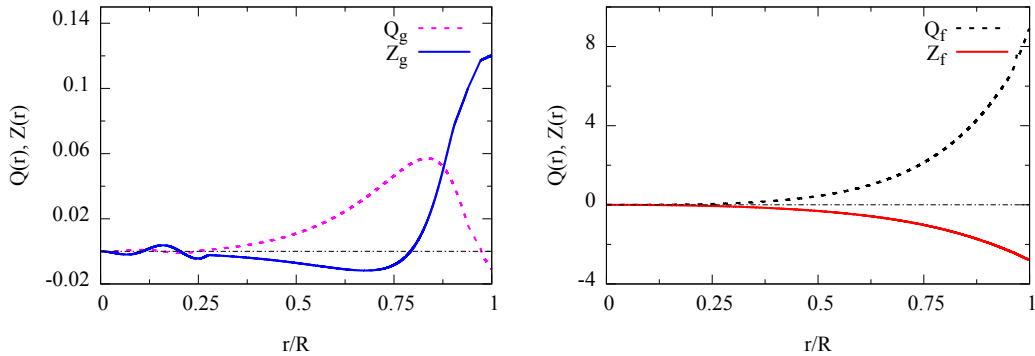


Figure 14. The solutions for the fluid perturbation functions $Q(r)$ and $Z(r)$, for the hybrid star of mass $M = 2.27M_\odot$ as a function of radial distance. The NL3 parameterized EOS is taken for hadronic matter while NJL model is taken for the quark matter EOS and Gibbs construction to find the mixed EOS. The left figure shows the perturbing functions associated with the g -modes while the right figure shows the same functions corresponding to f modes. The oscillatory behavior of $Z_g(r)$ near the core may be noted in the contrast to the Fig. 13

as at the surface as may be seen in Fig. 9 in contrast to the hadronic matter (relevant for NSs) for which it becomes significant only near the surface. Therefore there are additional nodes for Z_g in case of HSs as compared to NSs. This is also reflected in the behaviour of the functions $Q(r)$ and $Z(r)$ as shown in the left figure. As was the case with NS, for g mode the dominating contribution arises from the second term of the parenthesis of equation Eq. (3.40). The quantity in the parenthesis has a canceling effect on the other two terms in the Eq. (3.40). This leads to a slight oscillatory behaviour for the functions $Z(r)$ depending upon whether $Z'(r)$ is positive or negative up to r_c . Beyond it, ω_{BV} becomes significant only near the surface and the behaviour of $Z(r)$ and $Q(r)$ are similar to that of NS. In the right figure, we have shown the same functions for the f mode. The behaviour of these functions $Q(r)$ and $Z(r)$ associated to the f -modes are essentially similar to NSs.

6 Summary and conclusion

Let us summarize the salient features of the present investigation. We have looked into possible distinct features of HSs with a quark matter in the core and a NS without a quark matter in the core. This is investigated by looking into non-radial oscillations of compact stars. The EOS for HS is constructed using a RMF theory for nuclear matter and NJL model for quark matter. Gibbs criterion for MP is used to construct MP with two chemical potentials (μ_B and μ_E) imposing global charge neutrality condition. It is observed that the core of HSs can accommodate a mixture of nucleonic and quark matter, the pure quark matter phase being never achieved. In comparison to a NS without quark matter, the inclusion of MP of matter softens EOS, resulting in lower values for the maximum masses and bigger corresponding radii. Determining the composition of NS through observables it is necessary to break the degeneracy between normal and hybrid star. To this end, we looked into non-radial oscillation modes of such compact stars for this purpose. Unlike M-R curves for which EOS is sufficient, the analysis of oscillation modes requires the speed of sound of the charge neutral matter. Using a MP structure, it is observed that the equilibrium speed of sound shoots up at the transition between MP and HP in such a construct. It may be noted that

such a steep rise in the velocity of sound in a narrow region of density as one comes from the core towards the surface was also seen in a quarkyonic to hadronic matter transition [90] as well as in an EOS with ω condensate and fluctuations in pion condensate [91]. Such a steep rise in velocity in sound speed is generated naturally here through MP construct. This EOS is used to determine the frequencies of non-radial oscillations in NS within a relativistic Cowling approximation that neglects the fluctuation of the space time metric and results in a much simpler equation to solve and analyze. While this is not strictly consistent with the fully relativistic treatment, the impact of such simplified approximation is not severe, typically affecting the g modes at the 5 – 10% level while f modes are more sensitive to Cowling approximation [87]. Within the RMF model for nuclear matter, we estimated the f and g modes frequencies. The g mode solution for NS arises due to ω_{BV} when become significant towards the surface of NS. On the otherhand for HSs the ω_{BV} become significant near the core where the HQPT occurs. Due to the quark matter core both the ω_{BV} and g mode frequency get enhanced as compared to a normal NS.

We have focused our attention in the present investigation to non-radial oscillation modes corresponding to the quadruple fundamental modes and the gravity modes. In the presence of quark matter in a mixed phase with charge neutral nuclear matter, both these modes are enhanced with the effect being more for the g modes as compared to the high frequency f modes. The g modes that we have considered here are driven by nonvanishing Brunt-Väisälä frequency resulting from a chemical stratification and depends upon the compositional characteristics rather than a density discontinuity. This enhancement is due to the sharp drop of the equilibrium speed of sound at the on onset of the MP and is a distinct feature of HS as compared to a NS. In the context of gravitational wave from BNS merger, it is known that g modes can couple to tidal forces and can draw energy and angular momentum from the binary to the NS and cause an associated phase shift in gravitational wave signal [95]. With distinct enhancement of this mode for HS as compared to NS, one might expect a distinguishing signal from GW observations. However, the resulting phase shifts for NSs and HSs turns out to be similar order due to the longer merger times for the NSs [48]. Such conclusions are of course limited by the uncertainties arising from the value of tidal coupling. When these uncertainties are reduced through improved theoretical estimations, the high frequency g modes of HS can possibly be distinguished from those of NSs. The detection of g modes in BNS mergers by current detectors is challenging. Nonetheless, one hopes that with the third generation detectors like Einstein telescope or Cosmic explorer, one can possibly have direct detection of these modes and have conclusive signatures regarding the composition of the NS interior.

One of the novel feature of the present investigation has been the use of hadronic EOS modeled through RMF models with their parameters determined from the nuclear matter properties at saturation density with the NL3 parameterisation as well DDB parameterisation.

Unlike meta models [48], mean field model EOS are derived from a microscopic model described in terms of nucleons and mesons and quite successful in describing various properties of finite nuclei as well as NSs. The derivation for ω_{BV} as described here is rather general and can be used for any mean field model for nuclear/hyperonic matter. Similarly for quark matter NJL model is used which captures the important features of chiral symmetry breaking in strong interactions. It may be noted that these models can be extended to include strange quark matter. The calculational method developed here can be applied to the various other sophisticated models like 3 flavour NJL model, quark-meson model or Polyakov loop extension of such model describing the quark matter.

We have given in some detail the derivation of the relativistic pulsating equations involving Brunt-Väisälä frequency in which such a MP EOS as derived here. In addition we have discussed the behavior of the fluid perturbing functions in some details both with and without the HQPT which adds an understanding of the enhancement of oscillation frequencies for HSs. In future we would like to include the effects of the strange quarks in quark matter sector and correspondingly hyperons in the hadronic sector. It will also be interesting and important to include the effects of strong magnetic field for the structure of NSs [92] and its effect on the non-radial oscillation modes. We have focused our attention for NSM which is at zero temperature and vanishing a neutrino chemical potential. However, to study the proto-neutron stars we should take into account the thermal effects on the oscillations including the effects of neutrino trapping on the phase structure of matter. This will be relevant for the studying the oscillation modes from merging NS and detecting in future experimental facilities like advanced LIGO/Virgo and Einstein telescope.

Acknowledgments

The authors gratefully acknowledge discussions with P. Jaikumar, Bharat Kumar and their useful suggestions.

References

- [1] Luciano Rezzolla, Pierre Pizzochero, David Ian Jones, Nanda Rea, and Isaac Vidaña, editors. *The Physics and Astrophysics of Neutron Stars*, volume 457. Springer, 2018. doi: 10.1007/978-3-319-97616-7.
- [2] P. Haensel, A. Y. Potekhin, and D. G. Yakovlev. *Neutron stars 1: Equation of state and structure*, volume 326. Springer, New York, USA, 2007. doi: 10.1007/978-0-387-47301-7.
- [3] James M. Lattimer. The nuclear equation of state and neutron star masses. *Ann. Rev. Nucl. Part. Sci.*, 62:485–515, 2012. doi: 10.1146/annurev-nucl-102711-095018.
- [4] James M. Lattimer and Madappa Prakash. The Equation of State of Hot, Dense Matter and Neutron Stars. *Phys. Rept.*, 621:127–164, 2016. doi: 10.1016/j.physrep.2015.12.005.
- [5] M. Oertel, M. Hempel, T. Klähn, and S. Typel. Equations of state for supernovae and compact stars. *Rev. Mod. Phys.*, 89(1):015007, 2017. doi: 10.1103/RevModPhys.89.015007.
- [6] Gordon Baym, Tetsuo Hatsuda, Toru Kojo, Philip D. Powell, Yifan Song, and Tatsuyuki Takatsuka. From hadrons to quarks in neutron stars: a review. *Rept. Prog. Phys.*, 81(5):056902, 2018. doi: 10.1088/1361-6633/aaae14.
- [7] Anna L. Watts et al. Colloquium : Measuring the neutron star equation of state using x-ray timing. *Rev. Mod. Phys.*, 88(2):021001, 2016. doi: 10.1103/RevModPhys.88.021001.
- [8] Feryal Özel and Paulo Freire. Masses, Radii, and the Equation of State of Neutron Stars. *Ann. Rev. Astron. Astrophys.*, 54:401–440, 2016. doi: 10.1146/annurev-astro-081915-023322.
- [9] B. P. Abbott et al. GW170817: Measurements of neutron star radii and equation of state. *Phys. Rev. Lett.*, 121(16):161101, 2018. doi: 10.1103/PhysRevLett.121.161101.
- [10] Emmanuel Fonseca et al. The NANOGrav Nine-year Data Set: Mass and Geometric Measurements of Binary Millisecond Pulsars. *Astrophys. J.*, 832(2):167, 2016. doi: 10.3847/0004-637X/832/2/167.
- [11] John Antoniadis et al. A massive pulsar in a compact relativistic binary. *Science*, 340(6131), 2013. ISSN 0036-8075. doi: 10.1126/science.1233232. URL <http://science.sciencemag.org/content/340/6131/1233232>.

- [12] E. Fonseca et al. Refined Mass and Geometric Measurements of the High-mass PSR J0740+6620. *Astrophys. J. Lett.*, 915(1):L12, 2021. doi: 10.3847/2041-8213/ac03b8.
- [13] Roger W. Romani, D. Kandel, Alexei V. Filippenko, Thomas G. Brink, and WeiKang Zheng. PSR J1810+1744: Companion Darkening and a Precise High Neutron Star Mass. *Astrophys. J. Lett.*, 908(2):L46, 2021. doi: 10.3847/2041-8213/abe2b4.
- [14] Thomas E. Riley et al. A *NICER* View of PSR J0030+0451: Millisecond Pulsar Parameter Estimation. *Astrophys. J. Lett.*, 887(1):L21, 2019. doi: 10.3847/2041-8213/ab481c.
- [15] M. C. Miller et al. PSR J0030+0451 Mass and Radius from *NICER* Data and Implications for the Properties of Neutron Star Matter. *Astrophys. J. Lett.*, 887(1):L24, 2019. doi: 10.3847/2041-8213/ab50c5.
- [16] Thomas E. Riley et al. A *NICER* View of the Massive Pulsar PSR J0740+6620 Informed by Radio Timing and XMM-Newton Spectroscopy. *Astrophys. J. Lett.*, 918(2):L27, 2021. doi: 10.3847/2041-8213/ac0a81.
- [17] M. C. Miller et al. The Radius of PSR J0740+6620 from *NICER* and XMM-Newton Data. *Astrophys. J. Lett.*, 918(2):L28, 2021. doi: 10.3847/2041-8213/ac089b.
- [18] Tyler Gorda, Aleksii Kurkela, Paul Romatschke, Matias Säppi, and Aleksii Vuorinen. Next-to-Next-to-Next-to-Leading Order Pressure of Cold Quark Matter: Leading Logarithm. *Phys. Rev. Lett.*, 121(20):202701, 2018. doi: 10.1103/PhysRevLett.121.202701.
- [19] S. Borsányi, Z. Fodor, J. N. Guenther, R. Kara, S. D. Katz, P. Parotto, A. Pásztor, C. Ratti, and K. K. Szabó. Lattice QCD equation of state at finite chemical potential from an alternative expansion scheme. *Phys. Rev. Lett.*, 126(23):232001, 2021. doi: 10.1103/PhysRevLett.126.232001.
- [20] D. T. Son and M. A. Stephanov. Qcd at finite isospin density. *Phys. Rev. Lett.*, 86:592–595, Jan 2001. doi: 10.1103/PhysRevLett.86.592. URL <https://link.aps.org/doi/10.1103/PhysRevLett.86.592>.
- [21] D. Ebert and K. G. Klimenko. Pion condensation in electrically neutral cold matter with finite baryon density. *Eur. Phys. J. C*, 46:771–776, 2006. doi: 10.1140/epjc/s2006-02527-5.
- [22] A. Barducci, R. Casalbuoni, Giulio Pettini, and L. Ravagli. A Calculation of the QCD phase diagram at finite temperature, and baryon and isospin chemical potentials. *Phys. Rev. D*, 69:096004, 2004. doi: 10.1103/PhysRevD.69.096004.
- [23] Mark G. Alford, Krishna Rajagopal, and Frank Wilczek. QCD at finite baryon density: Nucleon droplets and color superconductivity. *Phys. Lett. B*, 422:247–256, 1998. doi: 10.1016/S0370-2693(98)00051-3.
- [24] Amruta Mishra and Hiranmaya Mishra. Chiral symmetry breaking, color superconductivity and color neutral quark matter: A Variational approach. *Phys. Rev. D*, 69:014014, 2004. doi: 10.1103/PhysRevD.69.014014.
- [25] Aman Abhishek and Hiranmaya Mishra. Chiral Symmetry Breaking, Color Superconductivity, and Equation of State for Magnetized Strange Quark Matter. *Springer Proc. Phys.*, 261:593–598, 2021. doi: 10.1007/978-981-33-4408-2_82.
- [26] Mark G. Alford, Krishna Rajagopal, and Frank Wilczek. Color flavor locking and chiral symmetry breaking in high density QCD. *Nucl. Phys. B*, 537:443–458, 1999. doi: 10.1016/S0550-3213(98)00668-3.
- [27] Massimo Mannarelli, Krishna Rajagopal, and Rishi Sharma. Testing the Ginzburg-Landau approximation for three-flavor crystalline color superconductivity. *Phys. Rev. D*, 73:114012, 2006. doi: 10.1103/PhysRevD.73.114012.
- [28] Krishna Rajagopal and Rishi Sharma. The Crystallography of Three-Flavor Quark Matter. *Phys. Rev. D*, 74:094019, 2006. doi: 10.1103/PhysRevD.74.094019.

- [29] David Radice, Albino Perego, Francesco Zappa, and Sebastiano Bernuzzi. GW170817: Joint constraint on the neutron star equation of state from multimessenger observations. *The Astrophysical Journal*, 852(2):L29, jan 2018. doi: 10.3847/2041-8213/aaa402. URL <https://doi.org/10.3847/2041-8213/aaa402>.
- [30] Tuhin Malik, N. Alam, M. Fortin, C. Providência, B. K. Agrawal, T. K. Jha, Bharat Kumar, and S. K. Patra. GW170817: constraining the nuclear matter equation of state from the neutron star tidal deformability. *Phys. Rev. C*, 98(3):035804, 2018. doi: 10.1103/PhysRevC.98.035804.
- [31] Cheng-Ming Li, Yan Yan, Jin-Jun Geng, Yong-Feng Huang, and Hong-Shi Zong. Constraints on the hybrid equation of state with a crossover hadron-quark phase transition in the light of GW170817. *Phys. Rev. D*, 98(8):083013, 2018. doi: 10.1103/PhysRevD.98.083013.
- [32] Jinniu Hu, Shishao Bao, Ying Zhang, Ken'ichiro Nakazato, Kohsuke Sumiyoshi, and Hong Shen. Effects of symmetry energy on the radius and tidal deformability of neutron stars in the relativistic mean-field model. *PTEP*, 2020(4):043D01, 2020. doi: 10.1093/ptep/ptaa016.
- [33] Soumi De, Daniel Finstad, James M. Lattimer, Duncan A. Brown, Edo Berger, and Christopher M. Biwer. Tidal Deformabilities and Radii of Neutron Stars from the Observation of GW170817. *Phys. Rev. Lett.*, 121(9):091102, 2018. doi: 10.1103/PhysRevLett.121.091102. [Erratum: *Phys.Rev.Lett.* 121, 259902 (2018)].
- [34] Katerina Chatziioannou, Carl-Johan Haster, and Aaron Zimmerman. Measuring the neutron star tidal deformability with equation-of-state-independent relations and gravitational waves. *Phys. Rev. D*, 97(10):104036, 2018. doi: 10.1103/PhysRevD.97.104036.
- [35] Vasileios Paschalidis, Kent Yagi, David Alvarez-Castillo, David B. Blaschke, and Armen Sedrakian. Implications from GW170817 and I-Love-Q relations for relativistic hybrid stars. *Phys. Rev. D*, 97(8):084038, 2018. doi: 10.1103/PhysRevD.97.084038.
- [36] Rana Nandi and Prasanta Char. Hybrid stars in the light of GW170817. *Astrophys. J.*, 857(1): 12, 2018. doi: 10.3847/1538-4357/aab78c.
- [37] Mark Alford, Matt Braby, M. W. Paris, and Sanjay Reddy. Hybrid stars that masquerade as neutron stars. *Astrophys. J.*, 629:969–978, 2005. doi: 10.1086/430902.
- [38] Wei Wei, Marc Salinas, Thomas Klähn, Prashanth Jaikumar, and Megan Barry. Lifting the Veil on Quark Matter in Compact Stars with Core g -mode Oscillations. *Astrophys. J.*, 904(2): 187, 2020. doi: 10.3847/1538-4357/abbe02.
- [39] V. A. Dommès and M. E. Gusakov. Oscillations of superfluid hyperon stars: decoupling scheme and g -modes. *Mon. Not. Roy. Astron. Soc.*, 455(3):2852–2870, 2016. doi: 10.1093/mnras/stv2408.
- [40] Hang Yu and Nevin N. Weinberg. Resonant tidal excitation of superfluid neutron stars in coalescing binaries. *Mon. Not. Roy. Astron. Soc.*, 464(3):2622–2637, 2017. doi: 10.1093/mnras/stw2552.
- [41] Bikram Keshari Pradhan and Debarati Chatterjee. Effect of hyperons on f -mode oscillations in Neutron Stars. *Phys. Rev. C*, 103(3):035810, 2021. doi: 10.1103/PhysRevC.103.035810.
- [42] Hajime Sotani, Nobutoshi Yasutake, Toshiki Maruyama, and Toshitaka Tatsumi. Signatures of hadron-quark mixed phase in gravitational waves. *Phys. Rev. D*, 83:024014, 2011. doi: 10.1103/PhysRevD.83.024014.
- [43] C. V. Flores and G. Lugones. Discriminating hadronic and quark stars through gravitational waves of fluid pulsation modes. *Class. Quant. Grav.*, 31:155002, 2014. doi: 10.1088/0264-9381/31/15/155002.
- [44] Alessandro Brillante and Igor N. Mishustin. Radial oscillations of neutral and charged hybrid stars. *EPL*, 105(3):39001, 2014. doi: 10.1209/0295-5075/105/39001.

- [45] Ignacio F. Ranea-Sandoval, Octavio M. Guilera, Mauro Mariani, and Milva G. Orsaria. Oscillation modes of hybrid stars within the relativistic Cowling approximation. *JCAP*, 12:031, 2018. doi: 10.1088/1475-7516/2018/12/031.
- [46] M. C. Rodriguez, I. F. Ranea-Sandoval, M. Mariani, M. G. Orsaria, G. Malfatti, and O. M. Guilera. Hybrid stars with sequential phase transitions: the emergence of the g_2 mode. *JCAP*, 02:009, 2021. doi: 10.1088/1475-7516/2021/02/009.
- [47] Shu Yan Lau and Kent Yagi. Probing hybrid stars with gravitational waves via interfacial modes. *Phys. Rev. D*, 103(6):063015, 2021. doi: 10.1103/PhysRevD.103.063015.
- [48] Prashanth Jaikumar, Alexandra Semposki, Madappa Prakash, and Constantinos Constantinou. g -mode oscillations in hybrid stars: A tale of two sounds. *Phys. Rev. D*, 103(12):123009, 2021. doi: 10.1103/PhysRevD.103.123009.
- [49] Kip S. Thorne and Alfonso Campolattaro. Non-Radial Pulsation of General-Relativistic Stellar Models. I. Analytic Analysis for $L \geq 2$. *ApJ*, 149:591, September 1967. doi: 10.1086/149288.
- [50] Steven L. Detweiler and L. Lindblom. On the nonradial pulsations of general relativistic stellar models. *Astrophys. J.*, 292:12–15, 1985. doi: 10.1086/163127.
- [51] Kostas D. Kokkotas and Bernd G. Schmidt. Quasinormal modes of stars and black holes. *Living Rev. Rel.*, 2:2, 1999. doi: 10.12942/lrr-1999-2.
- [52] Nils Andersson and Kostas D. Kokkotas. Towards gravitational wave asteroseismology. *Mon. Not. Roy. Astron. Soc.*, 299:1059–1068, 1998. doi: 10.1046/j.1365-8711.1998.01840.x.
- [53] P. N. McDermott, H. M. van Horn, and J. F. Scholl. Nonradial g -mode oscillations of warm neutron stars. *ApJ*, 268:837–848, May 1983. doi: 10.1086/161006.
- [54] Andreas Reisenegger and Peter Goldreich. Excitation of Neutron Star Normal Modes during Binary Inspiral. *ApJ*, 426:688, May 1994. doi: 10.1086/174105.
- [55] U. Lee and T. E. Strohmayer. Nonradial oscillations of rotating neutron stars: the effects of the Coriolis force. *Astronomy and Astrophysics*, v.311, p.155-171, 311:155–171, July 1996.
- [56] Reinhard Prix and Michel L. E. Rieutord. Adiabatic oscillations of non-rotating superfluid neutron stars. *Astron. Astrophys.*, 393:949–964, 2002. doi: 10.1051/0004-6361:20021049.
- [57] N. Andersson and G. L. Comer. On the dynamics of superfluid neutron star cores. *Mon. Not. Roy. Astron. Soc.*, 328:1129, 2001. doi: 10.1046/j.1365-8711.2001.04923.x.
- [58] Mikhail E. Gusakov and Elena M. Kantor. Thermal g -modes and unexpected convection in superfluid neutron stars. *Phys. Rev. D*, 88(10):101302, 2013. doi: 10.1103/PhysRevD.88.101302.
- [59] L. Gualtieri, E. M. Kantor, M. E. Gusakov, and A. I. Chugunov. Quasinormal modes of superfluid neutron stars. *Phys. Rev. D*, 90(2):024010, 2014. doi: 10.1103/PhysRevD.90.024010.
- [60] E. M. Kantor and M. E. Gusakov. Composition temperature-dependent g -modes in superfluid neutron stars. *Mon. Not. Roy. Astron. Soc.*, 442:90, 2014. doi: 10.1093/mnrasl/slu061.
- [61] A. Passamonti, N. Andersson, and W. C. G. Ho. Buoyancy and g -modes in young superfluid neutron stars. *Mon. Not. Roy. Astron. Soc.*, 455(2):1489–1511, 2016. doi: 10.1093/mnras/stv2149.
- [62] Hang Yu and Nevin N. Weinberg. Dynamical tides in coalescing superfluid neutron star binaries with hyperon cores and their detectability with third generation gravitational-wave detectors. *Mon. Not. Roy. Astron. Soc.*, 470(1):350–360, 2017. doi: 10.1093/mnras/stx1188.
- [63] P. B. Rau and I. Wasserman. Compressional modes in two-superfluid neutron stars with leptonic buoyancy. *Mon. Not. Roy. Astron. Soc.*, 481(4):4427–4444, 2018. doi: 10.1093/mnras/sty2458.

- [64] Constantinos Constantinou, Sophia Han, Prashanth Jaikumar, and Madappa Prakash. g modes of neutron stars with hadron-to-quark crossover transitions. *Phys. Rev. D*, 104(12):123032, 2021. doi: 10.1103/PhysRevD.104.123032.
- [65] Norman K. Glendenning. First order phase transitions with more than one conserved charge: Consequences for neutron stars. *Phys. Rev. D*, 46:1274–1287, 1992. doi: 10.1103/PhysRevD.46.1274.
- [66] Mark G. Alford, Krishna Rajagopal, Sanjay Reddy, and Frank Wilczek. The Minimal CFL nuclear interface. *Phys. Rev. D*, 64:074017, 2001. doi: 10.1103/PhysRevD.64.074017.
- [67] D. N. Voskresensky, M. Yasuhira, and T. Tatsumi. Charge screening at first order phase transitions and hadron quark mixed phase. *Nucl. Phys. A*, 723:291–339, 2003. doi: 10.1016/S0375-9474(03)01313-7.
- [68] Leticia F. Palhares and Eduardo S. Fraga. Droplets in the cold and dense linear sigma model with quarks. *Phys. Rev. D*, 82:125018, 2010. doi: 10.1103/PhysRevD.82.125018.
- [69] Marcus B. Pinto, Volker Koch, and Jorgen Randrup. The Surface Tension of Quark Matter in a Geometrical Approach. *Phys. Rev. C*, 86:025203, 2012. doi: 10.1103/PhysRevC.86.025203.
- [70] Bruno W. Mintz, Rainer Stiele, Rudnei O. Ramos, and Juergen Schaffner-Bielich. Phase diagram and surface tension in the three-flavor Polyakov-quark-meson model. *Phys. Rev. D*, 87(3):036004, 2013. doi: 10.1103/PhysRevD.87.036004.
- [71] G. Lugones, A. G. Grunfeld, and M. Al Ajmi. Surface tension and curvature energy of quark matter in the Nambu-Jona-Lasinio model. *PRC*, 88(4):045803, October 2013. doi: 10.1103/PhysRevC.88.045803.
- [72] N. Yasutake, R. Lastowiecki, S. Benic, D. Blaschke, T. Maruyama, and T. Tatsumi. Finite-size effects at the hadron-quark transition and heavy hybrid stars. *Phys. Rev. C*, 89:065803, 2014. doi: 10.1103/PhysRevC.89.065803.
- [73] D. N. Voskresensky, M. Yasuhira, and T. Tatsumi. Charge screening at first order phase transitions. *Phys. Lett. B*, 541:93–100, 2002. doi: 10.1016/S0370-2693(02)02186-X.
- [74] Toshiki Maruyama, Satoshi Chiba, Hans-Josef Schulze, and Toshitaka Tatsumi. Hadron-quark mixed phase in hyperon stars. *Phys. Rev. D*, 76:123015, 2007. doi: 10.1103/PhysRevD.76.123015.
- [75] S. Typel and H.H. Wolter. Relativistic mean field calculations with density-dependent meson-nucleon coupling. *Nuclear Physics A*, 656(3):331–364, 1999. ISSN 0375-9474. doi: [https://doi.org/10.1016/S0375-9474\(99\)00310-3](https://doi.org/10.1016/S0375-9474(99)00310-3). URL <https://www.sciencedirect.com/science/article/pii/S0375947499003103>.
- [76] Tuhin Malik and Constança Providência. Bayesian inference of signatures of hyperons inside neutron stars. *Phys. Rev. D*, 106(6):063024, 2022. doi: 10.1103/PhysRevD.106.063024.
- [77] Tuhin Malik, Márcio Ferreira, B. K. Agrawal, and Constança Providência. Relativistic Description of Dense Matter Equation of State and Compatibility with Neutron Star Observables: A Bayesian Approach. *Astrophys. J.*, 930(1):17, 2022. doi: 10.3847/1538-4357/ac5d3c.
- [78] J. D. Walecka. A Theory of highly condensed matter. *Annals Phys.*, 83:491–529, 1974. doi: 10.1016/0003-4916(74)90208-5.
- [79] J. Boguta and A. R. Bodmer. Relativistic Calculation of Nuclear Matter and the Nuclear Surface. *Nucl. Phys.*, A292:413–428, 1977. doi: 10.1016/0375-9474(77)90626-1.
- [80] J. Boguta and Horst Stoecker. Systematics of Nuclear Matter Properties in a Nonlinear Relativistic Field Theory. *Phys. Lett.*, 120B:289–293, 1983. doi: 10.1016/0370-2693(83)90446-X.

- [81] Brian D. Serot and John Dirk Walecka. Recent progress in quantum hadrodynamics. *Int. J. Mod. Phys.*, E6:515–631, 1997. doi: 10.1142/S0218301397000299.
- [82] Amruta Mishra, P. K. Panda, and W. Greiner. Vacuum polarization effects in hyperon rich dense matter: A Nonperturbative treatment. *J. Phys. G*, 28:67–83, 2002. doi: 10.1088/0954-3899/28/1/305.
- [83] Laura Tolos, Mario Centelles, and Angels Ramos. The Equation of State for the Nucleonic and Hyperonic Core of Neutron Stars. *Publications of the Astronomical Society of Australia*, 34:e065, 2017. doi: 10.1017/pasa.2017.60.
- [84] Laura Tolos, Mario Centelles, and Angels Ramos. EQUATION OF STATE FOR NUCLEONIC AND HYPERONIC NEUTRON STARS WITH MASS AND RADIUS CONSTRAINTS. *The Astrophysical Journal*, 834(1):3, dec 2016. doi: 10.3847/1538-4357/834/1/3. URL <https://doi.org/10.3847/1538-4357/834/1/3>.
- [85] Michael Buballa. Njl-model analysis of dense quark matter. *Physics Reports*, 407(4):205–376, 2005. ISSN 0370-1573. doi: <https://doi.org/10.1016/j.physrep.2004.11.004>. URL <https://www.sciencedirect.com/science/article/pii/S037015730400506X>.
- [86] Klaus Schertler, Stefan Leupold, and Jurgen Schaffner-Bielich. Neutron stars and quark phases in the NJL model. *Phys. Rev. C*, 60:025801, 1999. doi: 10.1103/PhysRevC.60.025801.
- [87] Pablo Gregorian. Nonradial neutron star oscillations. *A Master Thesis*, pages Universiteit Utrecht, Institute for theoretical physics, November 2014. URL <https://dspace.library.uu.nl/bitstream/handle/1874/306758/Master%20Thesis%20Theoretical%20Physics%2C%20Pablo%20Gregorian.pdf?sequence=2>.
- [88] M. Albright and J. I. Kapusta. Quasiparticle Theory of Transport Coefficients for Hadronic Matter at Finite Temperature and Baryon Density. *Phys. Rev. C*, 93(1):014903, 2016. doi: 10.1103/PhysRevC.93.014903.
- [89] Hajime Sotani, Kazuhiro Tominaga, and Kei-ichi Maeda. Density discontinuity of a neutron star and gravitational waves. *Phys. Rev. D*, 65:024010, 2002. doi: 10.1103/PhysRevD.65.024010.
- [90] Larry McLerran and Sanjay Reddy. Quarkyonic Matter and Neutron Stars. *Phys. Rev. Lett.*, 122(12):122701, 2019. doi: 10.1103/PhysRevLett.122.122701.
- [91] Robert D. Pisarski. Remarks on nuclear matter: How an ω_0 condensate can spike the speed of sound, and a model of $Z(3)$ baryons. *Phys. Rev. D*, 103(7):L071504, 2021. doi: 10.1103/PhysRevD.103.L071504.
- [92] N. K. Patra, Tuhin Malik, Debashree Sen, T. K. Jha, and Hiranmaya Mishra. An Equation of State for Magnetized Neutron Star Matter and Tidal Deformation in Neutron Star Mergers. *The Astrophysical Journal*, 900(1):49, 2020. doi: 10.3847/1538-4357/aba8fc.
- [93] G. Miniutti, J. A. Pons, E. Berti, L. Gualtieri, and V. Ferrari. Non-radial oscillation modes as a probe of density discontinuities in neutron stars. *MNRAS*, 338(2):389–400, January 2003. doi: 10.1046/j.1365-8711.2003.06057.x.
- [94] C. J. Krüger, W. C. G. Ho, and N. Andersson. Seismology of adolescent neutron stars: Accounting for thermal effects and crust elasticity. *Phys. Rev. D*, 92:063009, Sep 2015. doi: 10.1103/PhysRevD.92.063009. URL <https://link.aps.org/doi/10.1103/PhysRevD.92.063009>.
- [95] Dong Lai. Resonant oscillations and tidal heating in coalescing binary neutron stars. *Monthly Notices of the Royal Astronomical Society*, 270(3):611–629, 10 1994. ISSN 0035-8711. doi: 10.1093/mnras/270.3.611. URL <https://doi.org/10.1093/mnras/270.3.611>.